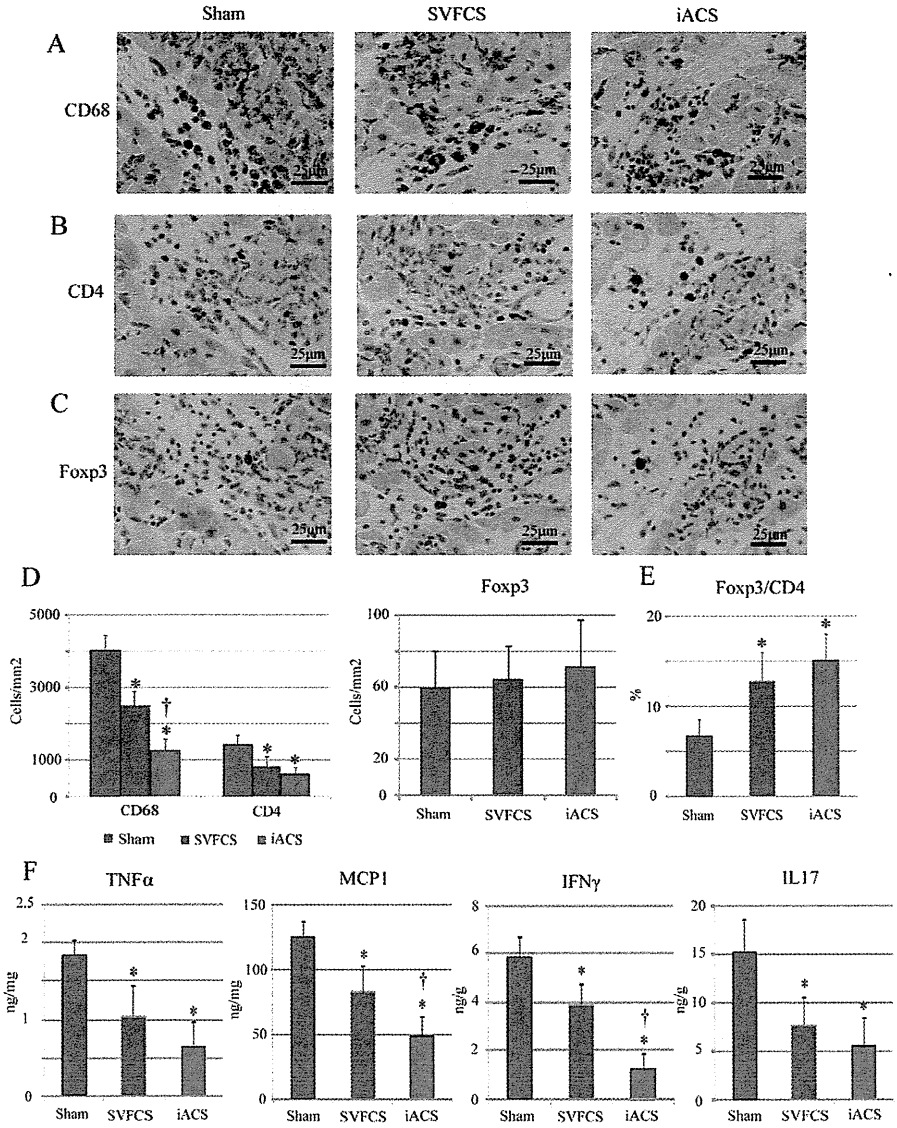

Figure 5. Induced adipocyte cell-sheet (iACS) suppressed the effector T-cell and macrophage responses, and promoted the regulatory T-cell response in experimental autoimmune myocarditis (EAM) rat heart. (**A–C**) Representative immunostaining for CD68 (**A**), CD4 (**B**), and Foxp3 (**C**) on postoperative day 14 in each group. (**D**) Quantification of CD68, CD4, and CD4/Foxp3-positive cells (n=12 each). CD68-positive macrophage accumulation in the myocardial interstitium was lowest in the iACS group followed by the stromal vascular-fraction cell-sheet (SVFCS) group compared to the Sham group ($P<0.001$, ANOVA). *$P<0.05$ vs. Sham, †$P<0.05$ vs. SVFCS. (**E**) Ratio of Foxp3-positive regulatory cells to CD4-positive T cells. *$P<0.05$ vs. Sham (n=12 each). (**F**) Myocardial tissues of EAM rat were homogenized and subjected to ELISA to detect tumor necrosis factor (TNF)α, monocyte chemotactic protein (MCP)1, interleukin (IL)17, and interferon (IFN)γ (n=12 each). *$P<0.05$ vs. Sham, †$P<0.05$ vs. SVFCS.

In addition, both dP/dt max and −dP/dt min were significantly greater in the iACS group than in the other groups (**Table S1**).

Discussion

We demonstrated here that iACS, which is generated from SVF isolated from subcutaneous fat tissues, extracellularly released a variety of cardioprotective factors including APN in vitro, and the released factors efficiently inhibited antigen-specific T-cell proliferation via the downregulation of IFNγ, IL17, and IL6 in vitro. Epicardially transplanted iACS supplied greater amounts of cardioprotective factors, such as APN, HGF or VEGF, into the inflamed myocardium of EAM rat hearts for at least 35 days, compared to the SVFCS transplantation or the Sham operation. Consequently, the iACS-transplanted EAM rat hearts showed less severe inflammation, lower expression levels of inflammatory cytokines, and a greater Foxp3-positive regulatory T-cell ratio, compared to the SVFCS-transplanted or Sham-operated EAM hearts. In addition, there was less progression of histological and functional LV remodeling in the EAM hearts following the iACS transplantation than after SVFCS transplantation or the Sham op-

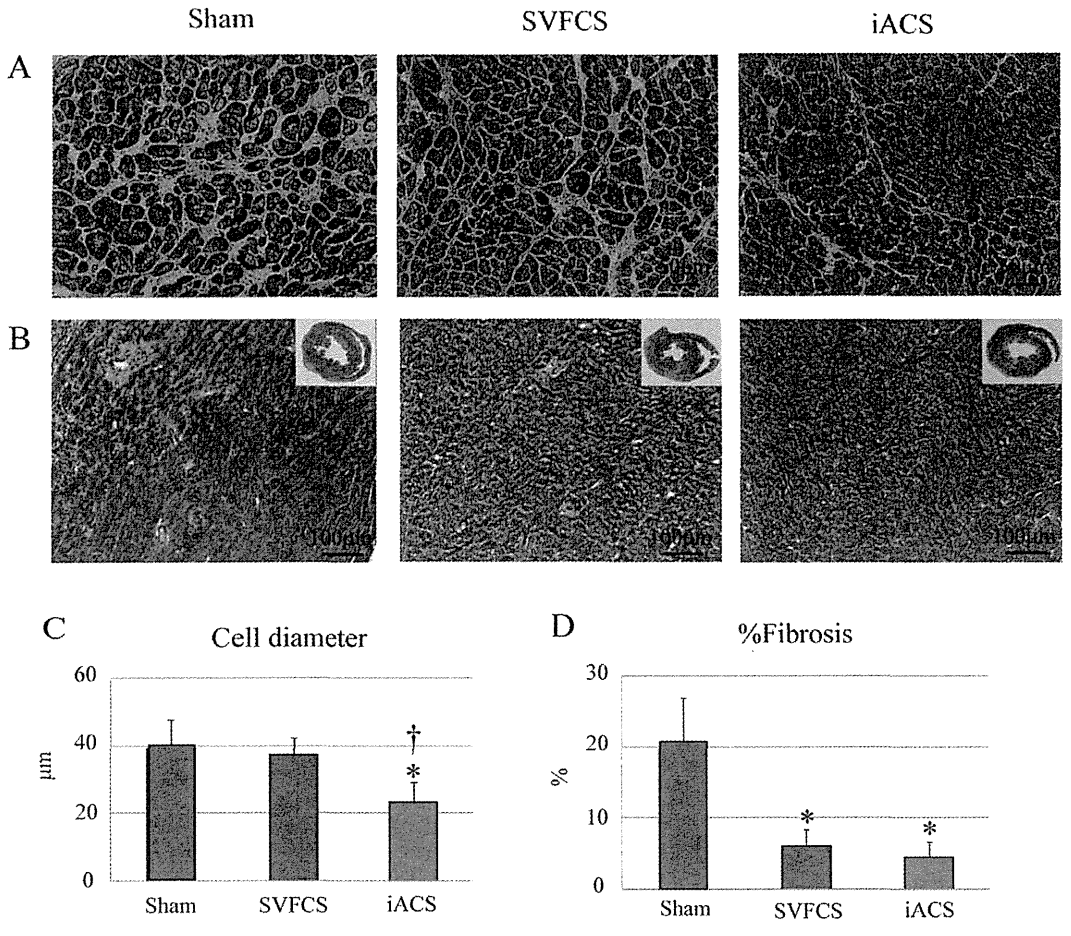

Figure 6. Effects of induced adipocyte cell-sheet (iACS) transplantation on left ventricular remodeling. (**A**,**B**) Representative hematoxylin-eosin staining (**A**) and Masson-trichrome staining (**B**) of the non-inflamed area on postoperative day 35 in each group. (**C**,**D**) Quantification of myocyte cell diameter (**C**) and percent fibrosis (**D**) (n=12 each). The myocyte diameter was significantly smaller in the iACS group than in the SVFCS and Sham groups (P<0.001, ANOVA), but the percentage of fibrosis was significantly lower in the iACS and the stromal vascular-fraction cell-sheet (SVFCS) groups than in the Sham group (P<0.001, Kruskal Wallis test). *P<0.05 vs. Sham, †P<0.05 vs. SVFCS.

eration.

Fat tissue is known to play a variety of important biological and physiological roles.[12,13] While bloated and/or degenerated fat tissues release inflammatory and atherogenic factors, intact normal fat tissues release protective factors represented by APN, which have anti-inflammatory/apoptotic/fibrotic effects on a variety of cardiac pathologies.[12–14] Importantly, protective factors, including APN, have been shown to be released by mature adipocytes, but not by undifferentiated ones such as SVF cells.[9] Because the cell culture of freshly isolated mature adipocytes and cell-sheet generation from these cells are technically difficult, we generated cell sheets containing mature adipocytes by inducing the cells in SVFCS to differentiate in vitro. We confirmed that both the iACS and SVFCS released little inflammation-related or atherogenic adipokines in vitro. In contrast, differentiated iACS but not SVFCS could secrete a large amount of APN.

Although the lifespan of adipocytes is generally shorter than that of SVF cells, SVF cells are known to appropriately and autonomously differentiate into adipocytes in vivo in adipose tissues in response to increased adipocyte cell death. Considering this reciprocal regulation between the 2 cell types, we ascertained that a minimum, rather than maximum, induction of differentiation might allow the iACS to provide APN to the host myocardium for a long time. In fact, iACS contained a certain amount of undifferentiated SVF cells before transplantation. While iACS supplied significantly more APN to EAM hearts than did SVFCS, the APN level in the inflamed myocardium was not different between the SVFCS-transplanted and Sham-operated hearts, suggesting that SVFCS did not release substantial APN after its transplantation into the heart. This contrary effect that SVF cells could differentiate into mature adipocytes in vitro, but not in vivo, could be explained by the different conditions for the differentiation from SVF cells to mature adipocytes. The appropriate induction of differentiation to iACS in vitro might have maintained the normal capacity of the adipocytes and/or SVF cells in the sheet to release abundant APN or other protective factors after transplantation, thereby eliciting the substantial therapeutic effects noted in this study.

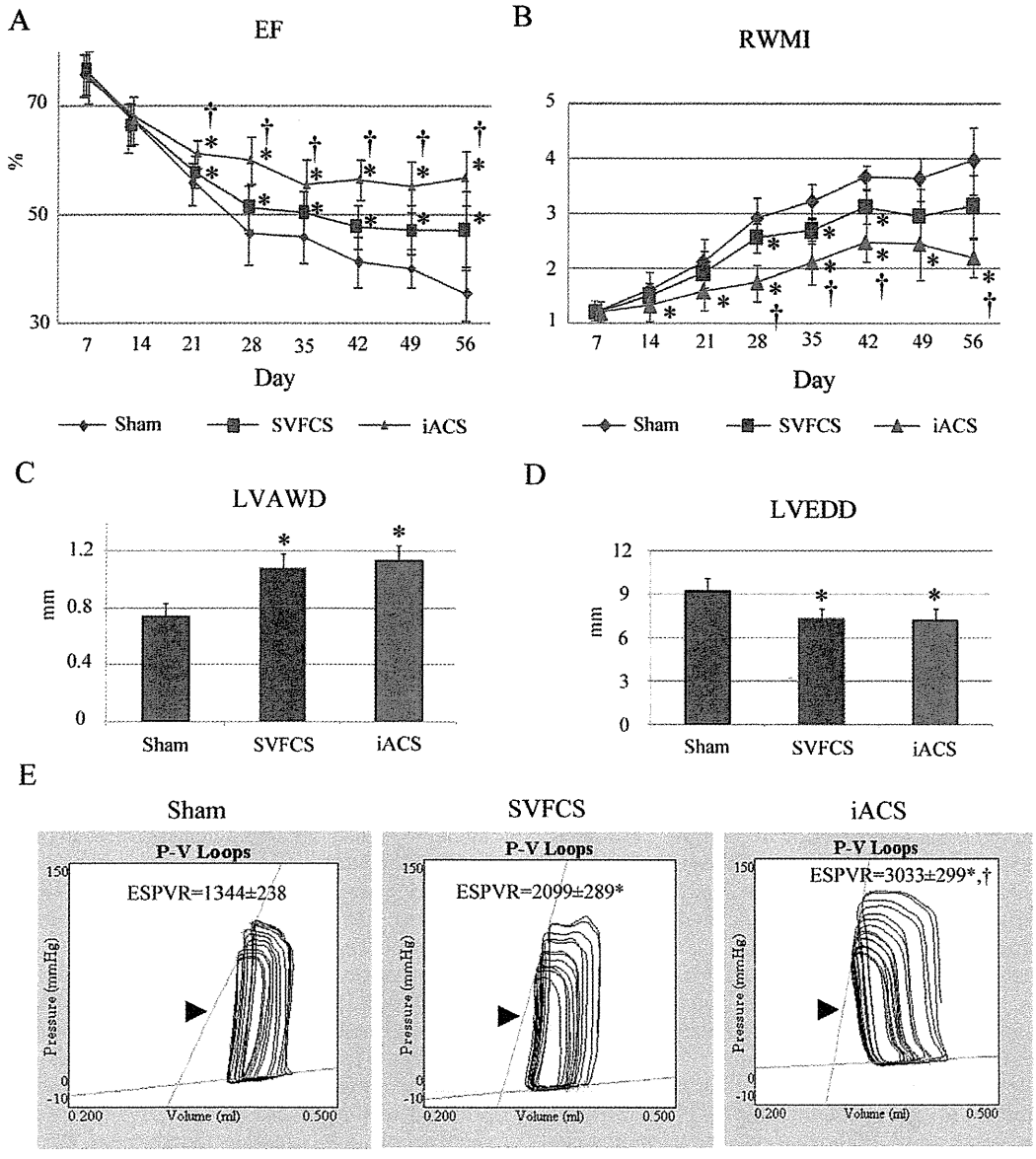

Figure 7. Cardiac structure and function after induced adipocyte cell-sheet (iACS) transplantation. (**A**,**B**) Serial echocardiographic parameters (**A**, ejection fraction [EF], **B**, regional wall motion index [RWMI]) in each group (day 7-day 42, n=12 each; day 49-day 56, n=6 each). The left ventricular (LV) EF was greatest in the iACS group, followed by the stromal vascular-fraction cell-sheet (SVFCS) group, then the Sham group (P<0.001, ANOVA). *P<0.05 vs. Sham, †P<0.05 vs. SVFCS. (**C**,**D**) LV anterior wall diameter (LVAWD) (**C**) and end-diastolic diameter (LVEDD) (**D**) on day 42 (n=12 each). LVEDD on day 42 was significantly lower in the iACS and SVFCS groups than in the Sham group (P<0.001, Kruskal-Wallis test). *P<0.05 vs. Sham. (**E**) Representative pressure-volume (P-V) loops on day 42 from each group (n=7 in each). Slopes indicate the end-systolic P-V relationship (ESPVR) (arrows). Representative P-V loops during inferior vena cava occlusion showed that the ESPVR was significantly greater in the iACS group than in the other groups (P<0.001, ANOVA). *P<0.05 vs. Sham, †P<0.05 vs. SVFCS.

The transplantation of either SVFCS or iACS resulted in positive pathological and functional effects on the EAM hearts in this study, although the impact was greater following iACS transplantation. The findings indicate that APN, which was more substantially increased in the iACS-transplanted hearts than in the SVFCS-transplanted ones, was a key factor accounting for the difference between the iACS and SVFCS treatments.[7] HGF and/or VEGF, which were increased in both the iACS and the SVFCS groups, have also been suggested to elicit therapeutic effects.[8]

Importantly, following iACS transplantation, both APN and HGF were present near CD4-positive effector T cells, which are known to express APN and HGF receptors,[7,8] suggesting that the upregulated APN and HGF might inhibit the accumulation of effector T cells and macrophages, and promote the accumulation of Foxp3 regulatory T cells, consequently at-

tenuating inflammation in the EAM hearts.

Treatment with ARB or PPARγ increases the circulating APN concentration in humans,[13] although these treatments are unlikely to deliver APN efficiently enough to the severely inflamed myocardium to be clinically relevant. Consistent with our results, previous reports demonstrated that the viral gene delivery of APN or HGF endogenously elevates its concentration in autoimmune myocarditis tissue, leading to immune-modulatory effects and the reversal of LV remodeling.[7,8] In contrast to the in vivo viral transfection method, our cell-sheet-based delivery system eliminates concerns related to the use of plasmid vectors and of needle injection into the host myocardium, and more efficiently delivers multiple cardioprotective factors over the long term.[9,15] After iACS implantation, the expression of cardioprotective factors (APN, HGF and VEGF) in the myocarditis tissues increased significantly, peaking at postoperative day 14, followed by stable and high expression through postoperative day 35. This prolonged and balanced delivery of cardioprotective factors might be more efficient and practical for clinical use than the one-time administration of a single reagent. Moreover, while the transplanted cells and their producing cytokines existed only in the epicardium, functional and pathological recovery by the iACS therapy was detected both in the inflamed and non-inflamed tissues, suggesting that the major therapeutic mechanisms in this study are not direct effects by transplanted cells but paracrine effects by host cardiac cells. The heart is generally formed in contractile myocardium, endocardium and epicardium, and the epicardium is thought to have a rich cardiac progenitor cell niche and to play an important role in cardiac repair.[16]

Notably, it has been shown that cell-sheet implantation into the epicardium induces the expression of multiple cardioprotective factors in the heart, and activates host epicardial cells crucial for cardiac repair. Therefore, these therapeutic effects in the study might be associated with the cell-sheet method. We believe that this "cross-talk" between the transplanted cells and the native myocardium activates and/or inhibits multiple pathways, leading to beneficial effects, and therefore that the cell-sheet method is a rational drug-delivery system for cardiac pathologies.

The T-cell-related immune modulatory effects were different between the EAM hearts treated with iACS vs. SVFCS transplantation in this study. While the level of Th1-producing IFNγ in the inflamed area of the heart on day 21 was lower in the iACS group than the SVFCS group, the level of Th17-produced IL17 was not significantly different between them. In addition, regulatory T cells accumulated prominently and to a similar degree in both the iACS and SVFCS groups. Nonetheless, the acute myocarditis severity on day 21 was significantly less after iACS implantation than after SVFCS implantation. The functional assessment also showed that the RWMI increase from day 7 to day 28 of the acute myocarditis phase was less in rats receiving iACS implantation than SVFCS implantation. Thus, the acute myocarditis severity on day 21 might be mainly associated with the Th1-mediated autoimmune response. In contrast, iACS implantation significantly elevated the level of APN in the myocarditis tissue, compared with SVFCS implantation. A T-cell proliferation assay showed that the addition of iACS supernatant, which contained APN and HGF, significantly decreased the level of Th1-producing IFNγ, compared with the addition of recombinant HGF alone. These findings indicated that the greater immunosuppressive effects of iACS implantation on effector Th1 cells compared with SVFCS implantation might be associated with the synergistic paracrine effects of APN and HGF released by the implanted iACS.

Regulatory T cells and effector Th17 cells might be reciprocally regulated in various autoimmune diseases.[3] In our study, some reciprocity between the number of accumulated Foxp3 regulatory T cells and the amount of IL17-producing Th17 in the myocarditis tissues was observed among the groups. ELISA analysis of the myocarditis tissues on day 21 showed that the iACS and SVFCS implantation similarly suppressed Th17 cells and activated the Foxp3 regulatory T cells. Recently, Baldeviano et al. reported that Th17-produced IL17 was dispensable for the severity of the acute myocarditis, but essential for the progression of cardiomyopathy.[3] Consistent with this, we found that the cardiac fibrosis related to LV remodeling in the chronic cardiomyopathy phase was similarly attenuated in the iACS and SVFCS implantation-treated rats via the suppression of profibrotic factors: TGFβ, MMP2, and MMP9. Thus, this inhibition of morphological deterioration might be associated with the suppression of the Th17-mediated autoimmune response and the induction of immune tolerance. In accordance with this scenario, morphological LV remodeling, such as LV dilatation and LV thinness, on day 42 was similarly suppressed in the groups receiving iACS and SVFCS implantation. In addition, the assessment of RWMI showed that the LV functional deterioration from day 28 to day 56 of the chronic cardiomyopathy phase was similarly suppressed in the rats receiving iACSs and SVFCSs, compared with the Sham operation. However, the cardiac hypertrophy on day 42 was attenuated only in the group receiving the iACSs. Several lines of evidence have indicated that APN directly affects injured myocytes via its receptor, eliciting anti-hypertrophic effects in a pressure-overload hypertrophic model.[13,17] Thus, the significant suppression of hypertrophy in iACS implantation-treated rats might have resulted from direct and synergistic effects of APN and HGF on the injured myocytes, and not from indirect immune modulatory effects via effector Th17 cells.

This study showed that iACS implantation had beneficial immunologic, pathologic, and functional effects on the heart of rats with autoimmune-associated myocarditis. However, in the clinical setting, fulminant myocarditis is etiologically highly heterogeneous, and thus, the autoimmune activity associated with it varies. The effectiveness of the iACS treatment shown in this study is therefore not directly translatable to the clinical situation. The investigation of T-cell activity by cardiac biopsy or circulating blood samples from patients with fulminant myocarditis might be useful for identifying responders or determining whether iACS treatment is indicated.

Normally, human myocarditis has a sudden onset and it has been known that it often follows a rapidly deteriorating course, leading to severe cardiac dysfunction. It has been reported that early diagnosis and subsequent treatment for fulminant myocarditis might be essential in clinical practice.[1] Therefore, methods need to be developed for promptly generating autologous iACS to maximize its therapeutic effects. The use of allogeneic iACS might be an option for clinical applications. Although there are immunologic concerns associated with the use of allogeneic iACS, this study suggested that iACS treatment upregulated APN and HGF, which attenuated the immunological response by inhibiting macrophages and activating regulatory T cells. Moreover, APN can limit allograft rejection by suppressing the expression of local cytokine/chemokine ligands that mediate inflammation and immune-cell recruitment.[18] Thus, the need for immunosuppressive medications might be minimal for allogeneic iACS treatment, although further study is needed.

Conclusions

This study clearly revealed that adipocyte-produced APN and HGF exert significant immunosuppressive effects, not only on Th1 cells, but also on Th17 cells in a typical model of autoimmune disorders. In addition, this tissue-engineered iACS improved the cardiac performance of autoimmune myocarditis via the suppression of autoimmune cellular activity, induction of immune-tolerance, and reversal of LV remodeling. This strategy of using a tissue-engineered drug-delivery system might be applicable to clinical treatments for fulminant myocarditis.

Acknowledgments

We thank Ms Masako Yokoyama and Mr Akima Harada for their technical assistance. We also thank Mr Norikazu Maeda and Mr Iichiro Shimomura for helpful discussions. This study was financially supported by a Grant-in-Aid from the Japan Society for the Promotion of Science (A22659251).

Disclosures

There were no competing interests.

References

1. Gupta S, Markham DW, Drazner MH, Mammen PP. Fulminant myocarditis. *Nat Clin Pract Cardiovasc Med* 2008; **5:** 693–706.
2. Cihakova D, Rose NR. Pathogenesis of myocarditis and dilated cardiomyopathy. *Adv Immunol* 2008; **99:** 95–114.
3. Baldeviano GC, Barin JG, Talor MV, Srinivasan S, Bedja D, Zheng D, et al. Interleukin-17A is dispensable for myocarditis but essential for the progression to dilated cardiomyopathy. *Circ Res* 2010; **106:** 1646–1655.
4. Yu F, Chen R, Takahashi T, Sumino H, Morimoto S, Nakahashi T, et al. Candesartan improves myocardial damage in obese mice with viral myocarditis and induces cardiac adiponectin. *Int J Cardiol* 2008; **129:** 414–421.
5. Choi JO, Yun SH, Sung K, Lee YT, Park JI, Ju ES, et al. Thioredoxin, adiponectin and clinical course of acute fulminant myocarditis. *Heart* 2011; **97:** 1067–1073.
6. Kunita E, Yamamoto H, Kitagawa T, Ohashi N, Utsunomiya H, Oka T, et al. Association between plasma high-molecular-weight adiponectin and coronary plaque characteristics assessed by computed tomography angiography in conditions of visceral adipose accumulation. *Circ J* 2012; **76:** 1687–1696.
7. Bobbert P, Scheibenbogen C, Jenke A, Kania G, Wilk S, Krohn S, et al. Adiponectin expression in patients with inflammatory cardiomyopathy indicates favourable outcome and inflammation control. *Eur Heart J* 2011; **32:** 1134–1147.
8. Futamatsu H, Suzuki J, Mizuno S, Koga N, Adachi S, Kosuge H, et al. Hepatocyte growth factor ameliorates the progression of experimental autoimmune myocarditis: A potential role for induction of T helper 2 cytokines. *Circ Res* 2005; **96:** 823–830.
9. Imanishi Y, Miyagawa S, Meaeda N, Fukushima S, Kitagawa-Sakakida S, Daimon T, et al. Induced adipocyte cell-sheet ameliorates cardiac dysfunction in a mouse myocardial infarction model: A novel drug delivery system for heart failure. *Circulation* 2011; **124**(Suppl 1)**:** S10–S17.
10. Lang RM, Bierig M, Devereux RB, Flachskampf FA, Foster E, Pellikka PA, et al. Recommendations for chamber quantification: A report from the American Society of Echocardiography's Guidelines and Standards Committee and the Chamber Quantification Writing Group, developed in conjunction with the European Association of Echocardiography, a branch of the European Society of Cardiology. *J Am Soc Echocardiogr* 2005; **18:** 1440–1463.
11. Eriksson U, Ricci R, Hunziker L, Kurrer MO, Oudit GY, Watts TH, et al. Dendritic cell-induced autoimmune heart failure requires cooperation between adaptive and innate immunity. *Nat Med* 2003; **9:** 1484–1490.
12. Robinson K, Prins J, Venkatesh B. Clinical review: Adiponectin biology and its role in inflammation and critical illness. *Crit Care* 2011; **15:** 221 (1–9).
13. Shibata R, Ouchi N, Murohara T. Adiponectin and cardiovascular disease. *Circ J* 2009; **73:** 608–614.
14. Yin WH, Wei J, Huang WP, Chen JW, Young MS, Lin SJ. Prognostic value of circulating adipokine levels and expressions of adipokines in the myocardium of patients with chronic heart failure. *Circ J* 2012; **76:** 2139–2147.
15. Shimizu T, Sekine H, Yamato M, Okano T. Cell sheet-based myocardial tissue engineering: New hope for damaged heart rescue. *Curr Pharm Des* 2009; **15:** 2807–2814.
16. Zhou B, Ma Q, Rajagopal S, Wu SM, Domian I, Rivera-Feliciano J, et al. Epicardial progenitors contribute to the cardiomyocyte lineage in the developing heart. *Nature* 2008; **454:** 109–113.
17. Shibata R, Ouchi N, Ito M, Kihara S, Shiojima I, Pimentel DR, et al. Adiponectin-mediated modulation of hypertrophic signals in the heart. *Nat Med* 2004; **10:** 1384–1389.
18. Okamoto Y, Christen T, Shimizu K, Asano K, Kihara S, Mitchell RN, et al. Adiponectin inhibits allograft rejection in murine cardiac transplantation. *Transplantation* 2009; **88:** 879–883.

Supplementary Files

Supplementary File 1

Supplementary Methods

Supplementary File 2

Table S1. Hemodynamic indices 5 weeks after the operation

Table S2. PCR primers used in real-time RT-PCR

Figure S1. T-cell proliferation assay.

Figure S2. Capillary formation on postoperative day 35 in each group.

Figure S3. Quantitative reverse transcription polymerase chain reaction (RT-PCR) results for profibrotic markers: TGFβ, TIMP1, TIMP2, TIMP3, MMP2, and MMP9, respectively (n=12 each).

Please find supplementary file(s);
http://dx.doi.org/10.1253/circj.CJ-14-0840

PLOS | ONE

N-Glycans: Phenotypic Homology and Structural Differences between Myocardial Cells and Induced Pluripotent Stem Cell-Derived Cardiomyocytes

Takuji Kawamura[1], Shigeru Miyagawa[1], Satsuki Fukushima[1], Akira Yoshida[2], Noriyuki Kashiyama[1], Ai Kawamura[1], Emiko Ito[1], Atsuhiro Saito[1], Akira Maeda[3], Hiroshi Eguchi[3], Koichi Toda[1], Jong-Kook Lee[2], Shuji Miyagawa[3], Yoshiki Sawa[1]*

1 Department of Cardiovascular Surgery, Osaka University Graduate School of Medicine, Suita, Osaka, Japan, **2** Department of Cardiovascular Regenerative Medicine, Osaka University Graduate School of Medicine, Suita, Osaka, Japan, **3** Division of Organ Transplantation, Department of Surgery, Osaka University Graduate School of Medicine, Suita, Osaka, Japan

Abstract

Cell surface glycans vary widely, depending on cell properties. We hypothesized that glycan expression on induced pluripotent stem cells (iPSCs) might change during cardiomyogenic differentiation toward the myocardial phenotype. *N*-glycans were isolated from iPSCs, iPSC-derived cardiomyocytes (iPSC-CM), and original C57BL/6 mouse myocardium (Heart). Their structures were analyzed by a mapping technique based on HPLC elution times and MALDI-TOF/MS spectra. Sixty-eight different *N*-glycans were isolated; the structures of 60 of these *N*-glycans were identified. The quantity of high-mannose type (immature) *N*-glycans on the iPSCs decreased with cardiomyogenic differentiation, but did not reach the low levels observed in the heart. We observed a similar reduction in neutral *N*-glycans and an increase in fucosylated or sialyl *N*-glycans. Some structural differences were detected between iPSC-CM and Heart. No *N*-glycolyl neuraminic acid (NeuGc) structures were detected in iPSC-CM, whereas the heart contained numerous NeuGc structures, corresponding to the expression of cytidine monophosphate-*N*-acetylneuraminic acid hydroxylase. Furthermore, several glycans containing Galα1-6 Gal, rarely identified in the other cells, were detected in the iPSC-CM. The expression of *N*-glycan on murine iPSCs changed toward the myocardial phenotype during cardiomyogenic differentiation, leaving the structural differences of NeuGc content or Galα1-6 Gal structures. Further studies will be warranted to reveal the meaning of the difference of *N*-glycans between the iPSC-CM and the myocardium.

Citation: Kawamura T, Miyagawa S, Fukushima S, Yoshida A, Kashiyama N, et al. (2014) *N*-Glycans: Phenotypic Homology and Structural Differences between Myocardial Cells and Induced Pluripotent Stem Cell-Derived Cardiomyocytes. PLoS ONE 9(10): e111064. doi:10.1371/journal.pone.0111064

Editor: Toru Hosoda, Tokai University, Japan

Received April 30, 2014; **Accepted** September 19, 2014; **Published** October 30, 2014

Data Availability: The authors confirm that all data underlying the findings are fully available without restriction. All relevant data are within the paper and its Supporting Information files.

Funding: YS received the funding to support this work from the Research Center Network for Realization of Regenerative Medicine managed by Centers for Clinical Application Research on Specific Disease/Organ and funded by Japan Science and Technology Agency. The funders had no role in study design, data collection and analysis, decision to publish, or preparation of the manuscript.

Competing Interests: The authors have declared that no competing interests exist.

* Email: sawa-p@surg1.med.osaka-u.ac.jp

Introduction

In vitro generation of cardiac myocytes by reprogramming is a promising technology in developing cell-transplant therapy for advanced cardiac failure [1] and drug discovery for a variety of cardiac diseases [2]. For both purposes, induced pluripotent stem cells (iPSCs) are most useful, since generation and cardiomyogenic differentiation of iPSCs has been standardized in human and a number of animals [3,4]. In fact, derivatives of iPSCs have been developed to the pre-clinical stage for cell transplantation therapy [5], while cardiac myocytes generated from patient-specific iPSCs have been studied to explore pathologic mechanisms and guide drug discovery [6,7]. However, cardiac myocyte preparations from iPSCs contain immature phenotypes, observed by electrophysiology, electron microscopy, and immunohistochemistry [8,9]; this may limit the safety and efficacy of cell transplantation therapy or reduce the accuracy and efficiency of drug discovery. The maturity of iPSC-derived cardiac myocytes (iPSC-CMs) has not been comprehensively or quantitatively evaluated.

Cell surface glycans have several important functions interacting with numerous proteins, including growth factors, morphogens and adhesion molecules, modulating dynamic cellular mechanisms such as cell-cell adhesion, cell activation, and malignant alterations [10–12]. In early mammalian embryos, associated with fertilization, some *N*-glycans play important roles of cell-cell adhesion [13–15]. In addition, cellular responsiveness to growth or arrest depends on total *N*-glycan number and the degree of branching of cell surface glycoproteins [16]. Furthermore, heparan sulfate, a kind of glycans, is required for embryonic stem cell (ESC) pluripotency, in particular lineage specification into mesoderm through facilitation of FGF and BMP signaling by stabilizing BMP ligand [17], leading the evidence that the expression patterns of cell surface glycans on ESCs changes during differentiation [18]. Thus, we hypothesized that cell surface glycan expression may

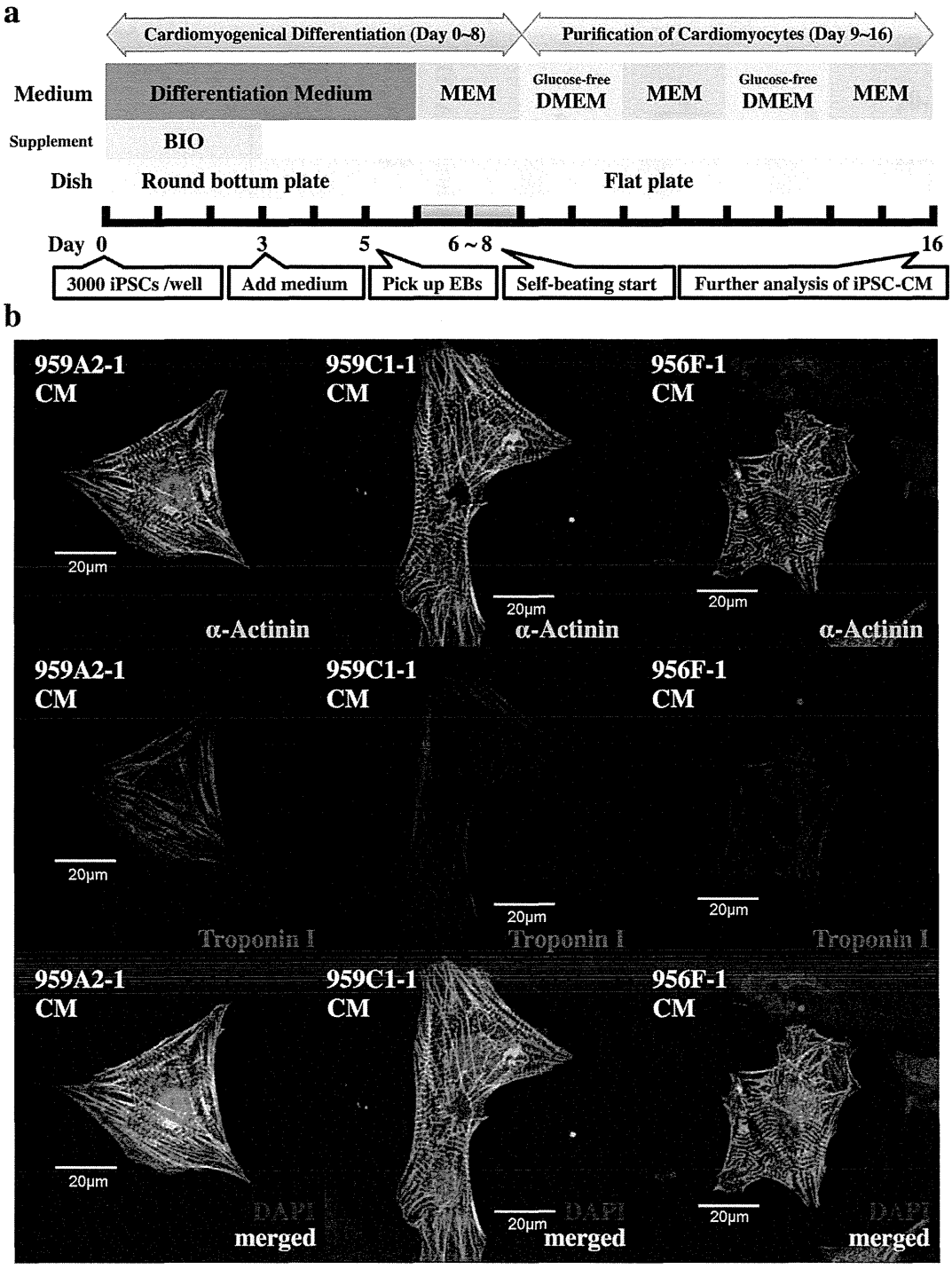

Figure 1. Cardiomyogenic differentiation of iPSCs and cardiomyocyte purification. (a) The cardiomyogenic differentiation protocol and cardiomyocyte purification process are illustrated. (b) IPSC-CMs stained with anti-α-actinin antibody (Alexa Fluor 488), anti-troponin I (Alexa Fluor 594) and DAPI, were analyzed with a confocal laser scanning microscopy. Abbreviations: EB, embryonic body; MEM, Modified Eagle's Medium; DMEM, Dulbecco's Modified Eagle's Medium; BIO, 6-bromoindirubin-3'-oxime.
doi:10.1371/journal.pone.0111064.g001

change during the course of cardiomyogenic differentiation of iPSCs *in vitro*. We analyzed *N*-glycan expression in undifferentiated iPSCs, iPSC-CMs, and adult murine myocardium by HPLC, to identify potential indicators of the maturity of differentiating cardiomyocytes from iPS cells *in vitro*.

Materials and Methods

Animal care procedures were consistent with the "Guide for the Care and Use of Laboratory Animals" (National Institutes of Health publication). Experimental protocols were approved by the

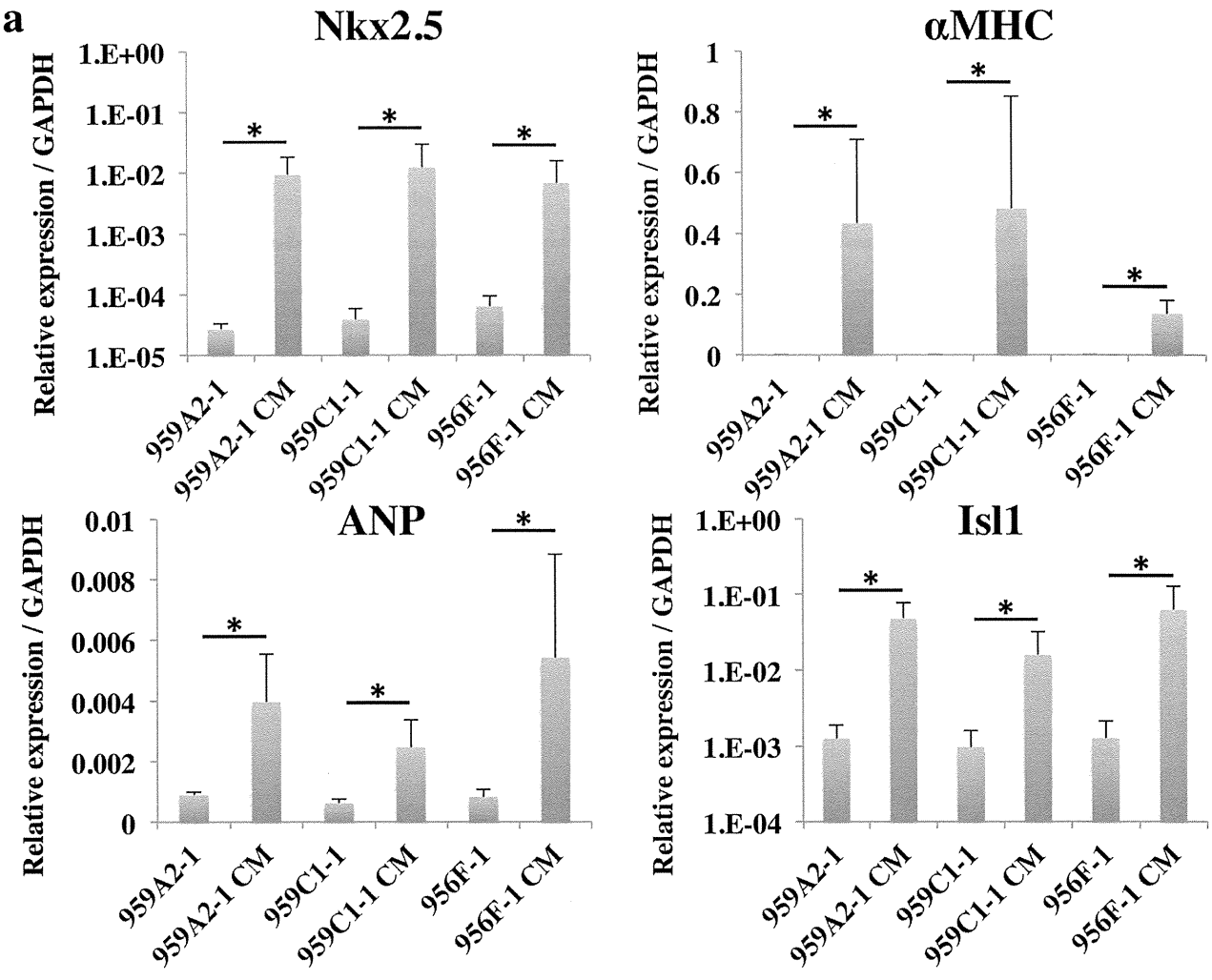
a
Nkx2.5
Relative expression / GAPDH
1.E+00
1.E-01
1.E-02
1.E-03
1.E-04
1.E-05
αMHC
1
0.8
0.6
0.4
0.2
0
ANP
0.01
0.008
0.006
0.004
0.002
0
Isl1
959A2-1
959A2-1 CM
959C1-1
959C1-1 CM
956F-1
956F-1 CM

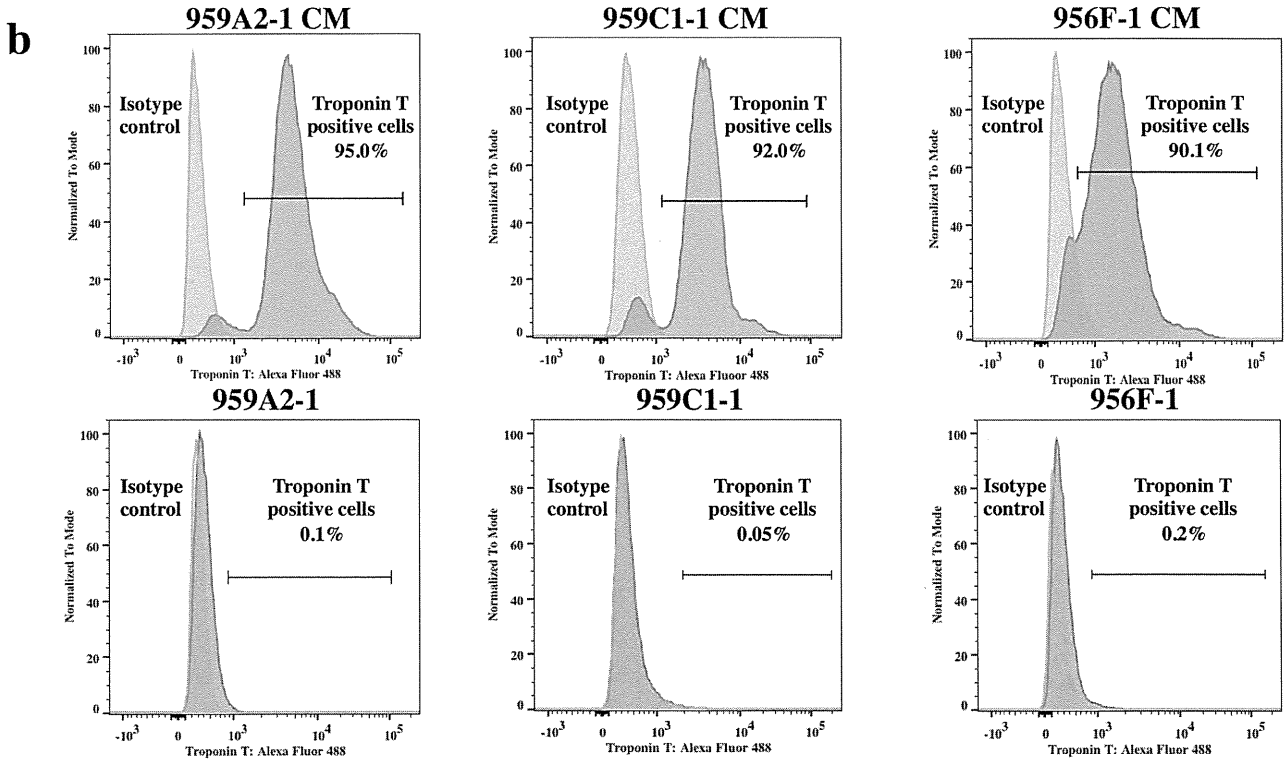
b
959A2-1 CM
959C1-1 CM
956F-1 CM
959A2-1
959C1-1
956F-1
Isotype control
Troponin T positive cells 95.0%
Troponin T positive cells 92.0%
Troponin T positive cells 90.1%
Troponin T positive cells 0.1%
Troponin T positive cells 0.05%
Troponin T positive cells 0.2%
Normalized To Mode
Troponin T: Alexa Fluor 488

Figure 2. Highly purified iPSC-CMs expressing cardiomyocyte marker genes. (a) Transcript expression of Nkx2.5, αMHC, ANP and Isl1 in the iPSCs and the iPSC-CMs were analyzed by real-time PCR. Results are expressed as the mean ± standard deviation. *P<0.05. (b) IPSC-CMs and iPSCs stained with anti-troponin T antibody or the isotype control, followed by Alexa Fluor 488-conjugated anti-mouse IgG antibody, were analyzed by flow cytometry.
doi:10.1371/journal.pone.0111064.g002

Ethics Review Committee for Animal Experimentation of Osaka University Graduate School of Medicine.

Cardiomyogenic differentiation of murine iPSCs *in vitro*

We used the murine iPSC lines, 959A2-1, 959C1-1, 956F-1 (generous gifts from Dr. Okita and Professor Yamanaka of the Center for iPS Cell Research and Application, Kyoto University, Kyoto, Japan). The cell lines were generated from C57BL/6 (B6) (CLEA) mouse embryonic fibroblasts by introducing *Oct3/4, Sox2, Klf4*, and *c-Myc* without viral vectors as described [19]. The iPSCs were cultured in the absence of serum and feeder cells by using ESGRO Complete PLUS Clonal Grade Medium (Millipore).

Cardiomyogenic differentiation of the iPSCs was performed as described [20,21], with modifications, followed by purification with glucose-free medium supplemented with lactic acid [22]; iPSCs (3×10^3) were resuspended in 100-μL aliquots of differentiation medium [DM; Dulbecco's Modified Eagle's Medium (DMEM; Nacalai Tesque) containing 15% fetal bovine serum (FBS; Biofill), 100 μmol/L non-essential amino acids (NEAA; Invitrogen), 2 mmol/L L-glutamine (Invitrogen), and 0.1 mmol/L 2-mercaptoethanol (Invitrogen)] containing 0.2 μmol/L 6-bromoindirubin-3′-oxime (BIO; a glycogen synthase kinase-3β inhibitor, to activate the Wnt-signaling pathway) (Calbiochem), and cultured in 96-well Corning Costar Ultra-Low attachment multiwell plates (Sigma-Aldrich) for 3 days. On day 3, an additional 100 μL DM without BIO was added to each well. On day 5, individual embryoid bodies (EBs) were transferred to 100-mm gelatin-coated dishes (250 EBs per dish). On days 6, 7, 10, 11, 14, and 15 the medium was exchanged for serum-free Modified Eagle's Medium (MEM; Invitrogen) with insulin transferrin-selenium-X (Invitrogen). On days 8, 9, 12, and 13, the medium was exchanged for Glucose-free DMEM (no glucose, no pyruvate, Invitrogen) supplemented with 4 mmol/L lactic acid (Wako Pure Chemical) for purification of cardiomyocytes. On day 16, the contracting cell clusters were used as cardiomyogenically differentiated iPSCs (959A2-1 CMs, 959C1-1 CMs, 956F-1 CMs: iPSC-CMs). The protocol and purification process are illustrated in Figure 1a.

Adult cardiac tissue from B6 mice (CLEA) was used as a control. Male B6 mice (8 weeks old) were sacrificed by intravenous administration of potassium chloride under inhalation anesthesia of isoflurane, and heart tissue from the left ventricle was harvested for further studies and labeled "Heart".

Immunohistochemistry analysis

IPSC-CMs were dissociated with 0.25% trypsin-EDTA and then fixed with 4% paraformaldehyde. The cells were stained with the following primary antibodies: mouse anti-α-actinin antibody (Sigma-Aldrich) and rabbit anti-troponin I antibody (Abcam), and then visualized by the following secondary antibodies: Alexa Fluor 488 donkey anti-mouse IgG (Invitrogen) and Alexa Fluor 594 goat anti-rabbit IgG (Invitrogen). The nucleus of the cells were stained with 4′, 6-Diamidino-2-phenylindole dihydrochloride (DAPI) and then observed with a confocal laser scanning microscopy FV1200 (Olympus).

Ca^{2+} transient measurement and pharmacological analysis

5 μM Fluo-8 regents (AAT Bioquest, Inc.) in serum-free MEM was added to iPSC-CMs after the cells were washed with phosphate buffered saline. The cells were incubated at 37°C for 30 min and then observed with a fluorescence microscopy. Fluorescence intensity of Fluo-8 dye was sequentially measured using iQ2 software (ANDOR) pre and post the administration of 1 μM isoproterenol.

Flow cytometry

IPSC-CMs were dissociated with 0.25% trypsin-EDTA and then fixed with CytoFix fixation buffer (BD) for 20 min. The cells were permeabilized with Perm/Wash buffer (BD) at room temperature for 10 min and then incubated with mouse anti-troponin T antibody (Thermo) for 30 min. Cells were washed with Perm/Wash buffer prior to incubation with the Alexa Fluor 488 rabbit anti-mouse IgG secondary antibody (Invitrogen) at room temperature for 30 min. These cells were analyzed on a FACS Canto II (BD).

Characterization of *N*-glycans derived from iPSCs, iPSC-CM, and Heart

All experimental procedures, including chromatography conditions and glycosidase treatments, have been described previously [23]. Cultured undifferentiated iPSCs, iPSC-CMs, and the heart tissue were treated with chloroform–methanol, then subjected to proteolysis with chymotrypsin and trypsin, followed by glycoamidase A digestion to release *N*-glycans. After removal of peptides, the reducing ends of the *N*-glycans were derivatized with 2-aminopyridine (Wako). This mixture was applied to a diethylaminoethyl (DEAE) column (Tosoh) or a TSK-gel Amide-80 column (Tosoh); each fraction from the amide column was then applied to a Shim-pack HRC-octadecyl silane (ODS) column (Shimadzu). The elution times of individual peaks from the amide-silica and ODS columns were normalized to a pyridylamino (PA)-derivatized isomalto-oligosaccharide with a known degree of polymerization, and are represented as glucose units (GU). Thus, each compound from these two columns provided a unique set of GU values, which corresponded to the coordinates of the 2D HPLC map. The PA-oligosaccharides were identified by comparison to the coordinates of ~500 reference PA-oligosaccharides in a homemade web application, GALAXY (http://www.glycoanalysis.info/galaxy2/ENG/index.jsp) [24]. The calculated HPLC map based on the unit contribution values was used to estimate some high-mannose type PA-oligosaccharides. The PA-oligosaccharides were co-chromatographed with the reference to PA-oligosaccharides on the columns to confirm their identities. PA-glycans that did not correspond to any of the *N*-glycans registered in GALAXY were trimmed by exoglycosidase to produce a series of known glycans [25].

Mass spectrometry

PA-oligosaccharides were analyzed by matrix-assisted laser desorption/ionization time-of-flight mass spectrometric (MALDI-TOF/MS). The matrix solution was prepared as follows: 10 mg of 2,5-Dihydroxybenzoic acid (Sigma) was dissolved in 1:1 (v/v)

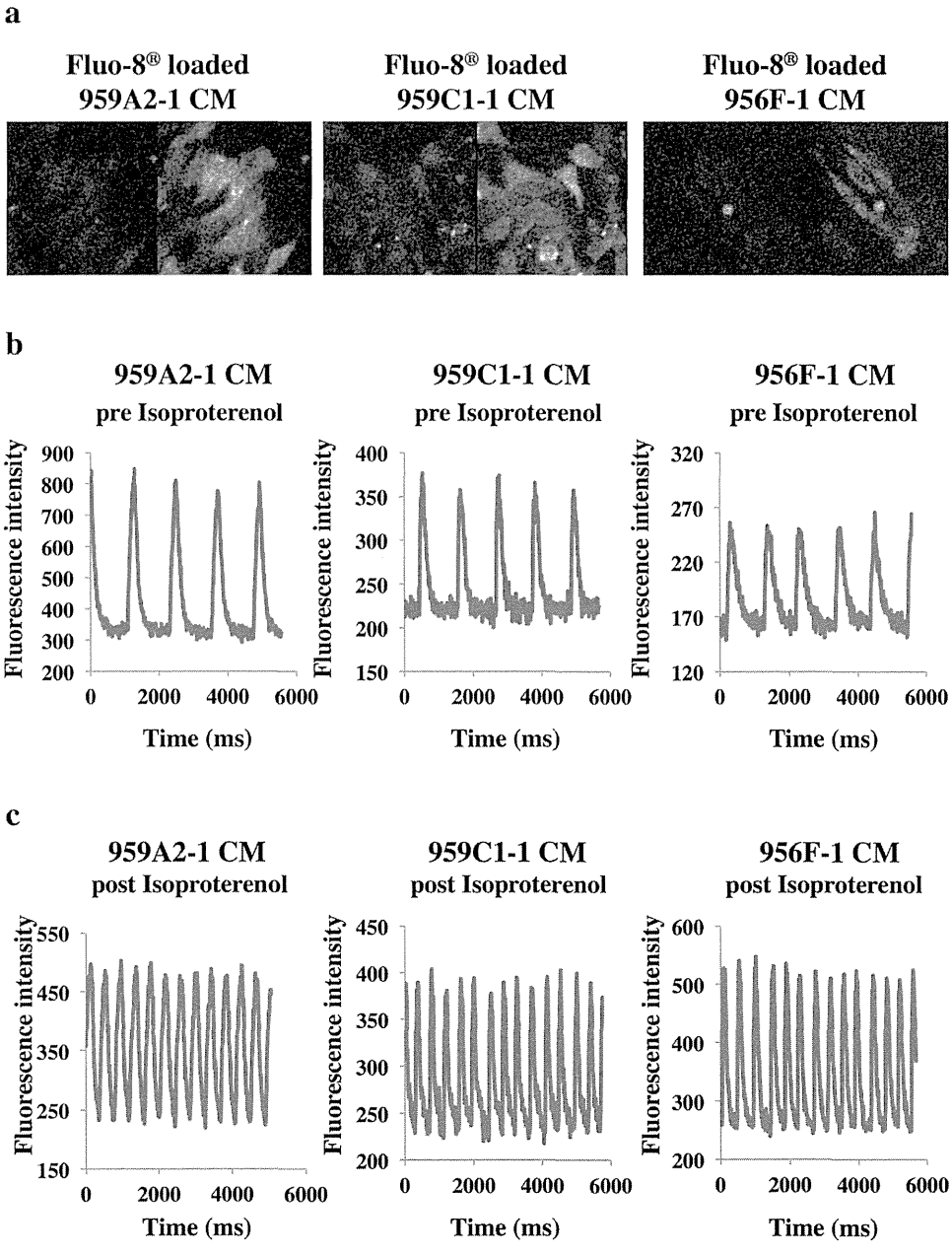

Figure 3. Ca^{2+} transient measurement of iPSC-CMs pre and post the administration of isoproterenol. (a) Fluo-8 loaded iPSC-CMs at the time of low (left) and high (right) fluorescence. (b), (c) Sequentially measured fluorescence intensity of Fluo-8 loaded iPSC-CMs pre (b) and post (c) the administration of 1 μM isoproterenol.
doi:10.1371/journal.pone.0111064.g003

acetonitrile/water (1 mL). Stock solutions of PA-glycans were prepared by dissolving them in pure water. One microliter of a sample solution was mixed on the target spot of a plate with 1 μL matrix solution and then allowed to air-dry. MALDI-TOF/MS data were acquired in the positive mode on an AXIMA-CFR (Shimadzu) operated in linear mode.

Materials

Glycoamidase A from sweet almond, α-mannosidase, β-galactosidase, and β-*N*-acetylhexosaminidase from jack bean were purchased from Seikagaku Kogyo (Tokyo, Japan). α-Galactosidase from coffee bean was purchased from Oxford GlycoSciences (Oxford, UK). Trypsin and chymotrypsin were obtained from Sigma (St. Louis, MO). Pronase protease from *Streptomyces griseus* was from Calbiochem (San Diego, CA). The pyridylamino (PA) derivatives of isomalto-oligosaccharides 4–20 (indicating the degree of polymerization of glucose residues) and reference PA-oligosaccharides were purchased from Seikagaku Kogyo.

Semi-quantitative PCR

DNA-free total RNA was extracted with the RNeasy RNA isolation Kit (Qiagen) and reverse-transcribed into cDNA using Omniscript reverse transcriptase (Qiagen), then analyzed by quantitative real-time PCR on an ABI PRISM 7700 thermocycler (Applied Biosystems) with the following TaqMan gene expression assays (Applied Biosystems): ST3Gal-III (Gal β1-3(4) GlcNAc α-2,

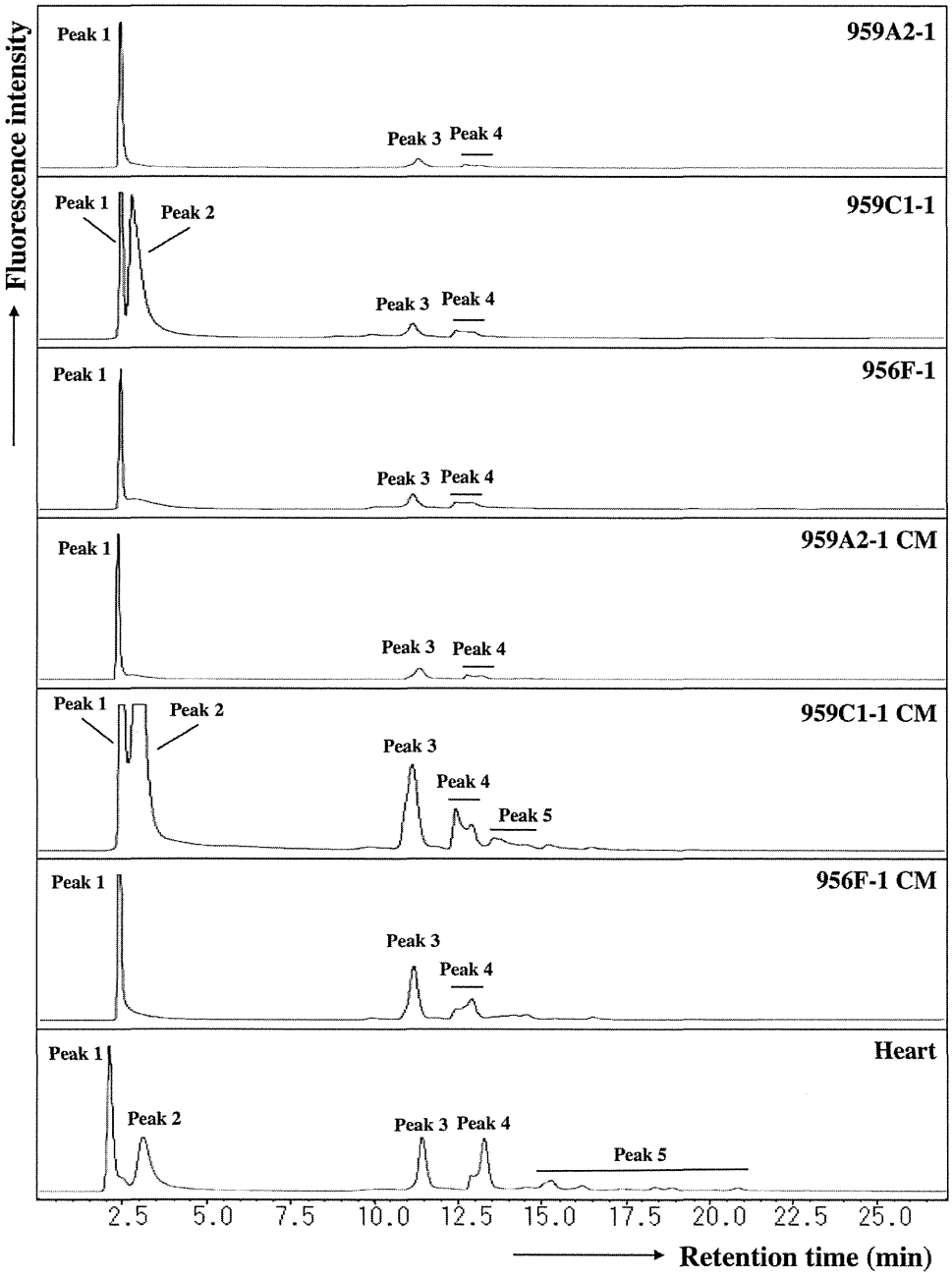

Figure 4. Anion-exchange DEAE elution profiles of PA-glycans. PA-glycans were fractionated according to their sialic acid content as neutral (peak 1), monosialyl (peak 3), and disialyl (peak 4) oligosaccharide fractions. Peaks 2 and 5 represent fractions containing no detectable PA-oligosaccharides.
doi:10.1371/journal.pone.0111064.g004

3-sialyltransferase), Mm00493353_m1; ST4Gal-IV (Gal β1-4(3) GlcNAc α-2, 3-sialyltransferase), Mm00501503_m1; ST6Gal-I (Gal β1-4 GlcNAc α-2, 6-sialyltransferase), Mm00486119_m1; CMAH (cytidine monophosphate-*N*-acetylneuraminic acid hydroxylase), Mm00483341_m1; GAPDH (glyceraldehyde-3-phosphate dehydrogenase), and Mm03302249_g1 and with SYBR Green dye (Applied Biosystems) using the following primers: Nkx2.5 F, 5′- CAAGTGCTCTCCTGCTTTCC -3′ R, 5′- GGCTTTGTCCAGCTCCACT -3′; αMHC (α-myosin heavy chain) F, 5′- GAGATTTCTCCAACCCAG -3′ R, 5′- TCTGACTTTCGGAGGTACT-3′; ANP (atrial natriuretic peptide) F, 5′- AAAGAAACCAGAGTGGGCAGAG -3′ R, 5′- CCAGGGTGATGGAGAAGGAG -3′; Isl1 F, 5′- TTTCCCTGTGTGTTGGTTGC -3′ R, 5′- TGATTACACTCCGCACATTTCA -3′; GAPDH F, 5′- CCAGTATGACTCCACTCACG -3′ R, 5′- GACTCCACGACATACTCAGC -3′. All experiments were performed by the relative standard curve method in three independent, triplicate experiments. Statistical comparison of the data was performed by Student's t-test.

Results

Highly purified cardiomyocytes derived from iPSCs

Cardiomyogenic differentiation was induced in murine iPSCs by using a slightly modified culture protocol (Figure 1a). The iPSC-CMs showed significantly higher expressions of Nkx2.5,

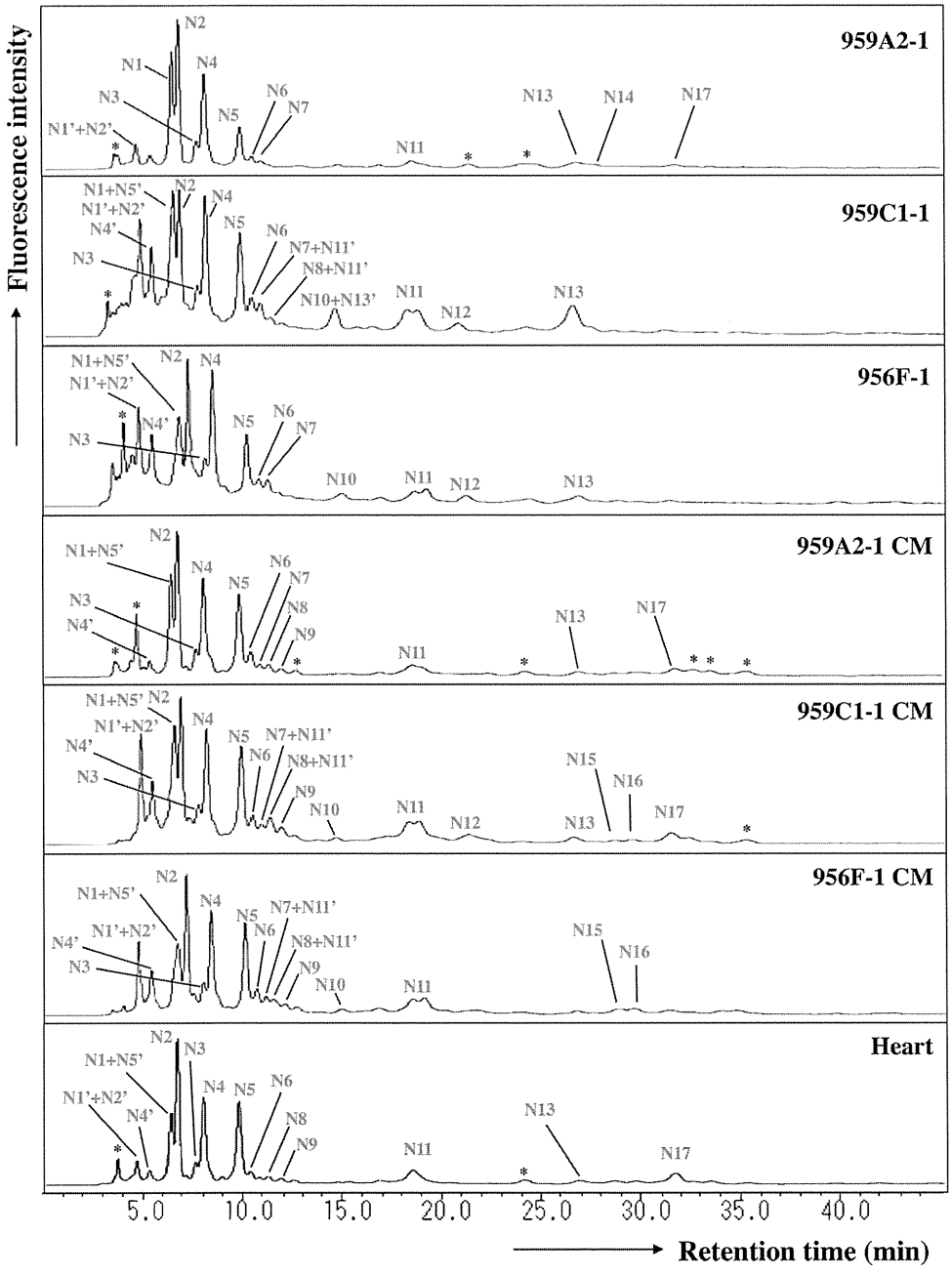

Figure 5. Reverse-phase ODS elution profiles of the neutral PA-glycans. The neutral fractions were individually applied to the ODS column and eluted according to their hydrophobicity. N1′, N2′, N4′, N5′ and N11′: epimerization of N1, N2, N4, N5 and N11. *Fractions containing no detectable PA-oligosaccharides.
doi:10.1371/journal.pone.0111064.g005

αMHC, ANP and Isl1 than undifferentiated iPSCs by semi-quantitative real-time PCR (Figure 2a), and showed sarcomere structures observed by immunohistological staining of α-actinin and troponin I (Figure 1b). The iPSC-CMs were functional with Ca^{2+} transient measurement (Figure 3a, b) and their beating rates were increased by the administration of isoproterenol (Figure 3c), meaning they had β-adrenergic receptors. Nearly all of the iPSC-CMs exhibited spontaneous and regular beating at room temperature (Video S1). The differentiation efficiency of murine iPSC was evaluated by flow cytometry analysis. More than 95% of the 959A2-1 CMs, 92% of the 959C1-1 CMs and 90% of the 956F-1 CMs were positive for troponin T (Figure 2b), while the undifferentiated iPSCs rarely expressed troponin T (Figure 2b).

N-Glycans isolated from iPSCs, iPSC-CM, and Heart

N-glycans extracted from undifferentiated iPSCs (959A2-1: 26 mg, 959C1-1: 11 mg and 956F-1: 10 mg of protein), iPSC-CM (959A2-1 CM: 15 mg, 959C1-1 CM: 12 mg and 956F-1 CM: 5.5 mg of protein), and the B6 heart muscle (82 mg of protein) were separated on a diethylaminoethyl (DEAE) column into five peaks, based on increasing acidity. Peak 1 represented a neutral (N) fraction, peak 3 a monosialyl (M) fraction, and peak 4 a disialyl

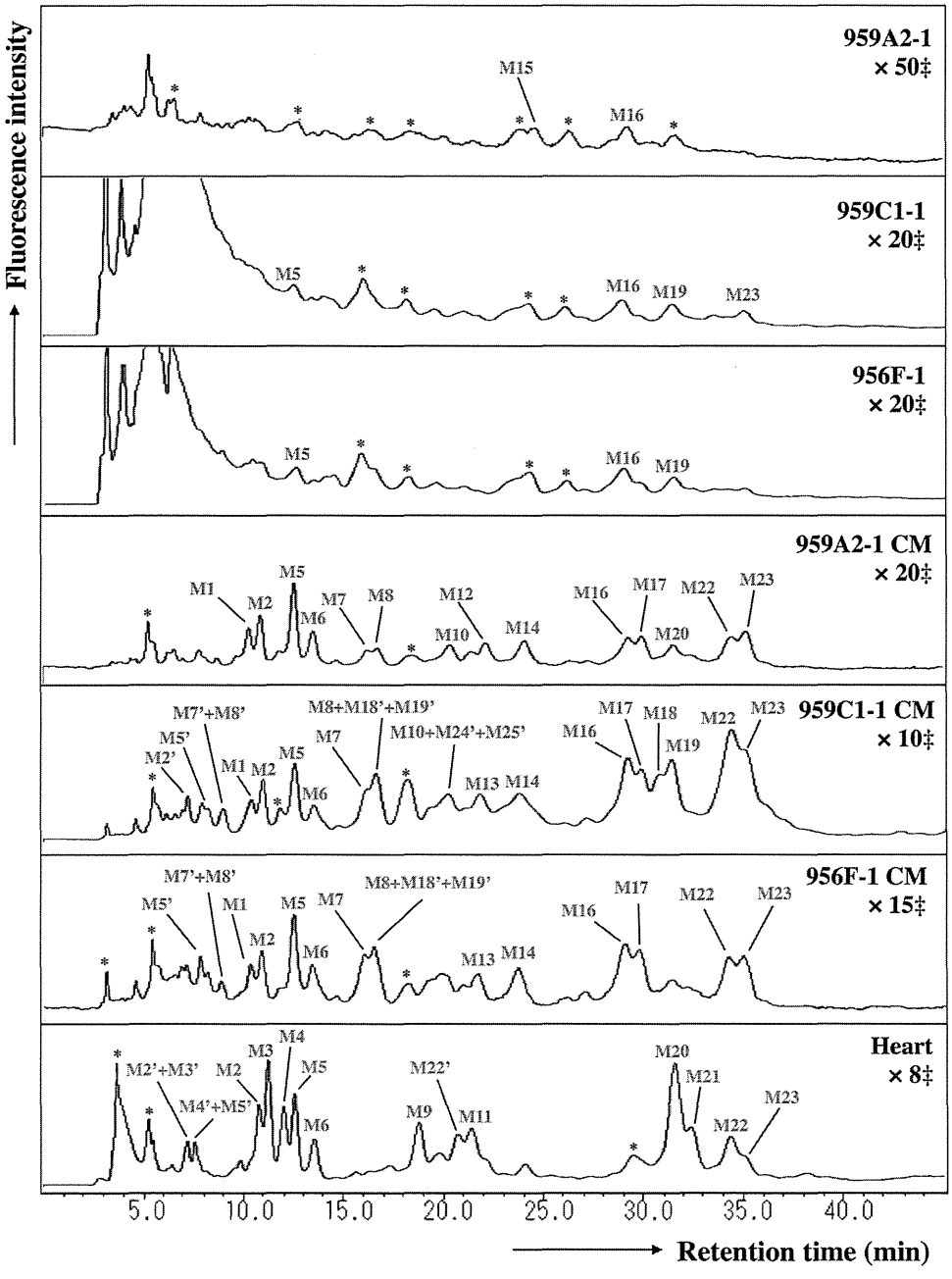

Figure 6. Reverse-phase ODS elution profiles of monosialyl PA-glycans. The monosialyl fractions were individually applied to the ODS column and eluted according to their hydrophobicity. M2′, M3′, M4′, M5′, M7′, M8′, M18′, M19′, M22′, M24′ and M25′: epimerization of M2, M3, M4, M5, M7, M8, M18, M19, M22, M24 and M25. *Fractions containing no detectable PA-oligosaccharides. ‡Magnification ratio to the fluorescence intensity of asialoglycan of each sample.
doi:10.1371/journal.pone.0111064.g006

(D) fraction. Glycan fractions in each of these peaks were as follows: iPSCs yielded 97% N, 0.5% M, 2.6% D (959A2-1), 98% N, 0.7% M, 1.1% D (959C1-1) and 96% N, 1.1% M, 3.1% D (956F-1) peak areas, iPSC-CMs yielded 89% N, 6.4% M, 4.4% D (959A2-1 CM), 79% N, 16% M, 4.8% D (959C1-1 CM) and 82% N, 10% M, 7.9% D (956F-1 CM) and Heart yielded 55% N, 19% M, and 25% D (Figure 4).

The ODS column separated the neutral fraction (Peak 1) into fractions N1–N17 (Figure 5), the monosialyl fraction (Peak 3) into fractions M1–M23 (Figure 6), and the disialyl fraction (Peak 4) into fractions D1–D12 (Figure 7). The signatures of each fraction differed between groups. These ODS fractions were individually fractionated on an amide column and analyzed by MALDI-TOF/MS. The N2, M6, M11, M14, M20, D4, D5, and D10 fractions contained two types of *N*-glycans, and the N6, N9, N11 and M2 fractions three types (data not shown). Thus, 68 different *N*-glycans were isolated from iPSCs, iPSC-CMs, and Heart.

Structures of *N*-Glycans isolated from iPSCs, iPSC-CM, and Heart

The isolated *N*-glycans were analyzed by means of a mapping technique based on their HPLC elution positions and MALDI-TOF/

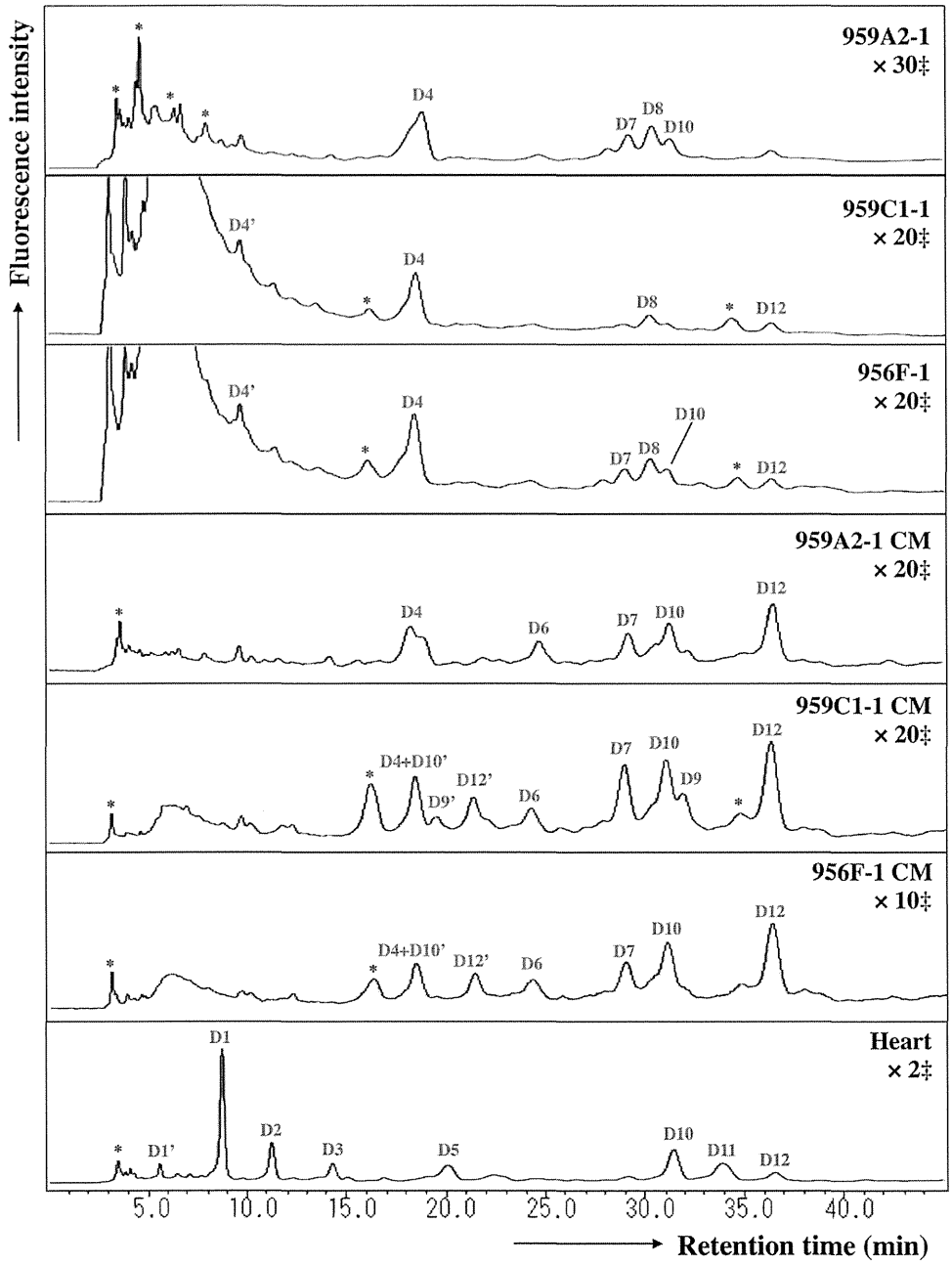

Figure 7. Reverse-phase ODS elution profiles of disialyl PA-glycans. The disialyl fractions were individually applied to the ODS column and eluted according to their hydrophobicity. D1′, D4′, D10′ and D12′: epimerization of D1, D4, D10 and D12; *Fractions containing no detectable PA-oligosaccharides. ‡Magnification ratio to the fluorescence intensity of asialoglycan of each sample.
doi:10.1371/journal.pone.0111064.g007

MS data. The coordinates of 54 *N*-glycans coincided with those for known references in the GALAXY database and their structures were identified. The coordinates for N9-3, M8, M11-2, M12, M13, M15, M17, M18, M19, M20-2, M21, M23, D8 and D9 did not correspond to known references.

N-glycans N9-2, M8, M12, M17, and M23 were trimmed by α-galactosidase but not by β-galactosidase or *N*-acetylglucosamidase. Their structures fit GALAXY references H5.12, 1A1-200.4, 1A3-200.4, 1A1-210.4, and 1A3-210.4, respectively. The galactosyl structures were then identified as Galα1-6Gal, because of the α-galactosidase-driven MS shifts. The structure of the M13 was identified by the coincidence with a GALAXY reference 1A2-H5.12 after being trimmed by α-L-fucosidase. The other *N*-glycans M11-2, M15, M18, M19, M20-2, M21, D8 and D9 were not identified in this study because they did not correspond to GALAXY references even after α-galactosidase digestions. They are described in Figure 8 and Table S1-S5 with their proposed formulas based on MALDI-TOF/MS data.

High-mannose *N*-Glycans were reduced by cardiomyogenic differentiation

The quantity of high-mannose *N*-glycans (HM) calculated from the total volume of N1–N6-2, N7 was highest in the iPSCs (959A2-1: 87.7%, 959C1-1: 68.3% and 956F-1: 78.2%), lower in the

Code No.	N1	N2-1	N2-2	N3	N4	N5	N6-1	N6-2	N6-3	N7	N8	N9-1
GU; ODS (Amid)	5.0 (8.8)	5.3 (7.9)	5.3 (9.5)	6.0 (7.8)	6.2 (7.0)	7.3 (6.0)	7.6 (4.2)	7.6 (5.0)	7.6 (4.6)	7.9 (3.3)	8.1 (7.3)	8.2 (5.6)
Mass (Da)	1800	1638	1962	1638	1475	1313	989	1151	1192	827	1679	1354
Structure	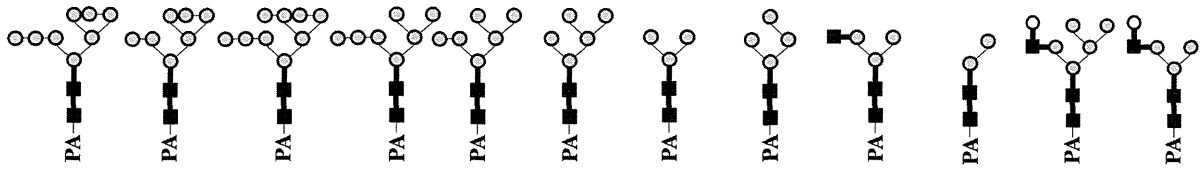											

N9-2	N9-3	N10	N11-1	N11-2	N11-3	N12	N13	N14	N15	N16	N17
8.2 (6.4)	8.3 (8.2)	9.3 (5.0)	10.5 (3.7)	10.5 (4.6)	10.5 (6.9)	11.2 (6.1)	12.8 (5.3)	13.0 (5.0)	13.3 (6.2)	13.5 (6.3)	14.2 (7.3)
1516	1841	1395	973	1135	1720	1500	1541	1338	1704	1704	1866
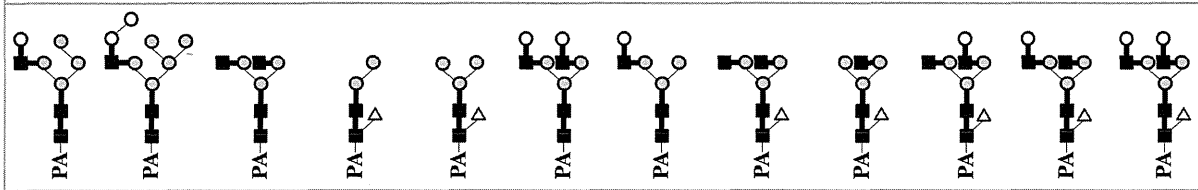											

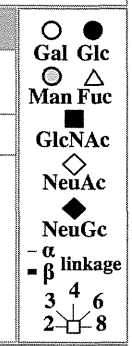

M1	M2-1	M2-2	M2-3	M3	M4	M5	M6-1	M6-2	M7	M8	M9	M10	M11-1	M11-2
7.6 (7.5)	7.9 (5.8)	7.9 (6.6)	7.9 (7.5)	8.1 (7.5)	8.4 (6.7)	8.6 (7.0)	9.0 (5.3)	9.0 (6.1)	10.1 (7.1)	10.3 (7.9)	10.6 (7.1)	11.0 (6.3)	11.3 (6.6)	11.3 (8.8)
1970	1646	1808	2027	1986	1824	1970	1646	1808	2011	2173	2027	1792	2011	2360
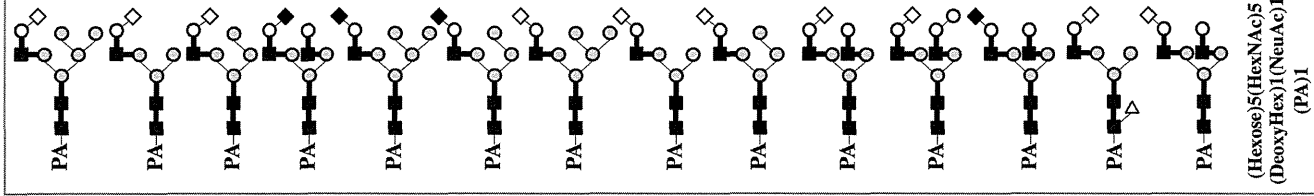														

M12	M13	M14-1	M14-2	M15	M16	M17	M18	M19	M20-1	M20-2	M21	M22	M23
11.5 (7.4)	11.3 (7.4)	11.8 (6.5)	11.8 (5.6)	12.1 (8.3)	13.3 (7.5)	13.7 (8.3)	13.8 (7.4)	14.0 (8.2)	14.2 (7.5)	14.2 (8.2)	14.5 (8.3)	15.1 (6.9)	15.3 (7.8)
2173	2116	1954	1792	2173	2157	2320	2360	2522	2173	2522	2344	2157	2320
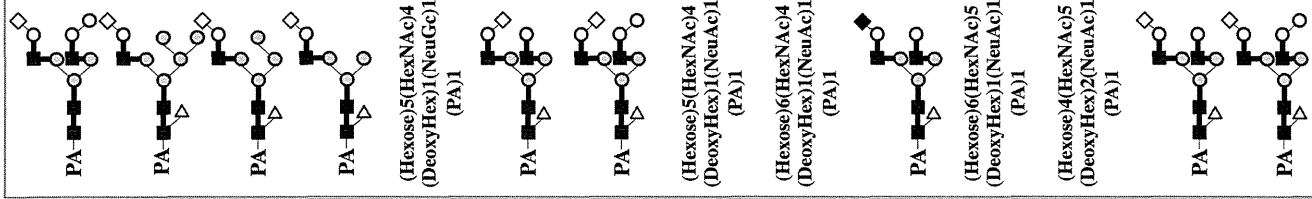													

D1	D2	D3	D4-1	D4-2	D5-1	D5-2	D6	D7	D8	D9	D10-1	D10-2	D11	D12
7.0 (8.2)	8.3 (7.8)	9.3 (8.6)	10.6 (6.9)	10.6 (7.3)	10.9 (7.4)	10.9 (8.1)	12.1 (6.4)	13.5 (7.7)	13.9 (6.8)	14.1 (7.5)	14.2 (7.2)	14.2 (7.7)	15.0 (7.2)	15.9 (6.7)
2334	2334	2480	2302	2302	2334	2480	2302	2448	2537	2854	2448	2480	2464	2448
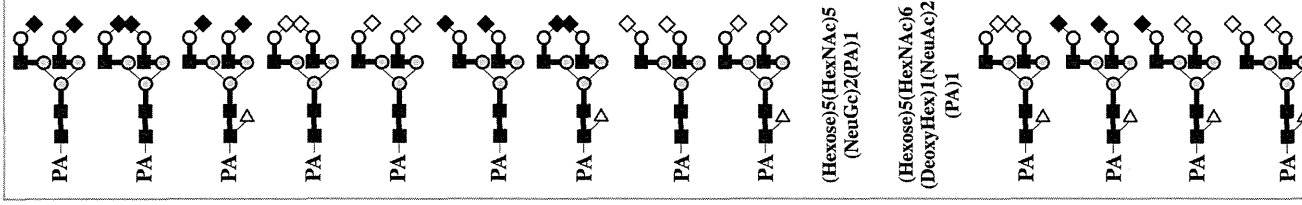														

Figure 8. Structures of neutral, monosialyl, and disialyl PA-oligosaccharides in iPSCs, iPSC-CM, and heart cells. Glucose units (GU) were calculated from the peak elution times for the ODS column in Figure 5, 6 and 7, and the amide column (data not shown). Average mass (Mass) calculated from the *m/z* values of $[M+Na]^+$ or $[M+H]^+$ ion for neutral, $[M-H]^-$ ion for monosialyl, and $[M-H]^-$ & $[M+Na-2H]^-$ ions for disialyl PA-oligosaccharides.
doi:10.1371/journal.pone.0111064.g008

iPSC-CMs (959A2-1 CM: 77.4%, 959C1-1 CM: 60.0% and 956F-1 CM: 65.1%), and lowest in the Heart (46.9%). The quantity of monofucosylated, difucosylated, and other types of *N*-glycans were greater in the iPSC-CMs and Heart (Figure 8, 9).

Sialyl *N*-glycans increased with cardiomyogenic differentiation

The quantity of monosialyl *N*-glycans (MS) calculated from the total volume of M1–M23 increased in iPSC-CMs (959A2-1 CM: 6.4%, 959C1-1 CM: 15.7% and 956F-1 CM: 10.5%) and Heart (19%) and were low in iPSCs (959A2-1: 0.5%, 959C1-1: 0.7% and 956F-1: 1.1%). The disialyl *N*-glycans (DS; D1–D12) yielded a similar pattern. The quantity of asialyl *N*-glycans (AS; N1–N17) decreased in iPSC-CMs (959A2-1 CM: 89.2%, 959C1-1 CM: 79.4% and 956F-1 CM: 81.7%) and Heart (55.3%) in comparison to the iPSCs (959A2-1: 96.9%, 959C1-1: 98.1% and 956F-1: 95.8%) (Figure 9, 10).

Rarely expressed *N*-glycans

The sialic acids identified in this study were either *N*-acetyl neuraminic acid (NeuAc) or *N*-glycolyl neuraminic acid (NeuGc). The quantity of monosialyl and disialyl *N*-glycans containing only NeuAc (A, A/A) was lowest in iPSCs (959A2-1: 2.5%, 959C1-1: 1.7% and 956F-1: 3.7%) and similar in iPSC-CMs (959A2-1 CM: 10.6%, 959C1-1 CM: 21% and 956F-1 CM: 18%) and the Heart (8%). The quantity of monosialyl and disialyl *N*-glycans containing only NeuGc (G, G/G) was markedly higher in the Heart (32.8%) than in iPSCs (959A2-1: 0.6%, 959C1-1: 0.1% and 956F-1: 0.5%) or iPSC-CMs (959A2-1 CM: 0%, 959C1-1 CM: 0% and 956F-1 CM: 0%) (Figure 10a).

Expression of glycosyl transferase, ST3Gal-III, ST3Gal-IV, ST6Gal-I, and CMAH in the iPSCs, iPSC-CMs, and Heart was assessed by RT-PCR to explore the glycan structures responsible for the differences between groups. The Heart expressed high levels of CMAH (0.91±0.13/GAPDH); levels in the iPSCs and iPSC-CMs were markedly lower (iPSCs: 959A2-1 0.011±0.0065/GAPDH, 959C1-1 0.013±0.0070/GAPDH, 956F-1 0.0045±0.0042/GAPDH, $P<0.05$; iPSC-CM: 959A2-1 CM 0.21±0.16/GAPDH, 959C1-1 CM 0.19±0.04, 956F-1 CM 0.45±0.31, $P<0.05$). Expression of ST3Gal-III was significantly higher in the Heart (0.98±0.13/GAPDH) than in iPSCs (959A2-1: 0.21±0.05/GAPDH, 959C1-1: 0.18±0.07/GAPDH, 956F-1: 0.27±0.05/GAPDH) and iPSC-CMs (959A2-1 CM: 0.40±0.10/GAPDH, 959C1-1 CM: 0.35±0.09/GAPDH, 956F-1 CM: 0.66±0.18); expression of ST3Gal-IV did not differ between groups. ST6Gal-I expression was significantly higher in iPSC-CMs (959A2-1 CM: 1.87±0.41/GAPDH, 959C1-1 CM: 1.95±0.22/GAPDH, 956F-1 CM: 3.08±1.27/GAPDH) than in iPSCs (959A2-1: 0.51±0.18/GAPDH, 959C1-1: 0.40±0.09/GAPDH, 956F-1: 0.62±0.29/GAPDH) and the Heart (1.04±0.13/GAPDH) (Figure 10b).

Discussion

Sixty-eight different *N*-glycans were isolated from iPSCs, iPSC-CMs, and the Heart. The structures of 60 *N*-glycans were identified, based on their HPLC elution peaks (Figure 8, Table S1-S5). Each preparation contained a combination of neutral, monosialyl, and disialyl *N*-glycans.

The molar ratios of high-mannose, monofucosylated, and difucosylated *N*-glycans were substantially different between groups (Figure 9), although no clear differences in the abundance of these glycans were found. The decrease in high-mannose *N*-glycans and increase of fucosylated *N*-glycans in iPSC-CMs versus iPSCs is consistent with a previous report on a comparison of ESC derived cardiomyocytes to undifferentiated ESCs [18]. Generally, all *N*-glycans are synthesized from the high-mannose type by a large array of sequentially and competitively acting biosynthetic enzymes located throughout the endoplasmic reticulum and Golgi apparatus [26], indicating that the high-mannose type of *N*-glycans could be categorized as a marker of immaturity. In this study, the high-mannose *N*-glycans were highest in the immature iPSC and lowest in the Heart, or mature tissue; thus, the quantity of high-mannose-type *N*-glycans might be an indicator of maturity in iPSC-derivatives and the iPSC-CMs in our protocol may still be immature in comparison to cardiac tissue.

Clear differences in glycan abundance were observed, such as hybrid and complex types represented by N9-1, N9-3, N15, N16, M1, M2-1, M2-2, M7, M8, M10, M12, M13, M14-1, M14-2, M17, M18, M20-2, D6 and D9 in iPSC-CMs, M2-3, M3, M4, M9, M11-1, M11-2, M20-1, M21, D1, D2, D3, D5-1, D5-2, D10-2 and D11 in Heart and N14 and M15 in iPSCs; these may also be indicators of maturation stage. In addition, expression of monosialyl and disialyl *N*-glycans in iPSC-CMs fell between the levels observed in the iPSCs and Heart, as were the molar ratios, indicating that the iPSC-CMs may still be immature stage. While many *N*-glycolyl neuraminic acid (NeuGc) structures were detected in the Heart, iPSCs and iPSC-CMs did not contain NeuGc in their sialyl structures, except for D8. Moreover, the molar ratio of NeuAc was low in iPSCs and iPSC-CMs. This finding is one of the clearest differences between iPSCs or iPSC-CMs and Heart cells.

The proposed spectra-based composition of the D8 glycans in iPSCs was [(Hexose)5(HexNAc)5(NeuGc)2(PA)1], indicating that it contains NeuGc. However, D8 might be quite a rare exception because transcript levels of CMAH, which catalyzes the conversion of NeuAc to NeuGc, was quite low in iPSCs in comparison to the Heart. This data suggests that during the process of reprograming, iPSCs suppress or eliminate CMAH activity. We conclude that iPSCs contain less sialic acid (especially NeuGc) and high-mannose structures are abundant in the *N*-glycans. In contrast, heart cells produce numerous sialyl-*N*-glycans, especially NeuGc. Transcript levels of CMAH tended to increase in iPSC-CMs relative to iPSCs, suggesting cardiomyogenic differentiation may induce expression of CMAH. If the iPSC-CMs could be matured more closely to the Heart by some additional methods of culture, the quantity of high mannose type of *N*-glycans might decrease more closely to the Heart, and might produce *N*-glycans containing NeuGc, followed by the expression of CMAH.

A terminal NeuGc, the Hanganutziu-Deicher (H-D) epitope [27], is widely distributed in the animal kingdom with the exception of humans and chickens. Expression of NeuGc is controlled by CMAH activity. Irie et al. [28] and Chou et al. [29] cloned the cDNA for human CMAH and reported that the *N*-terminal truncation of human CMAH is caused by deletion of Exon 6, a 92-base pair segment in the genomic DNA. Expression of this truncation in the heart eliminates NeuGc in sialyl

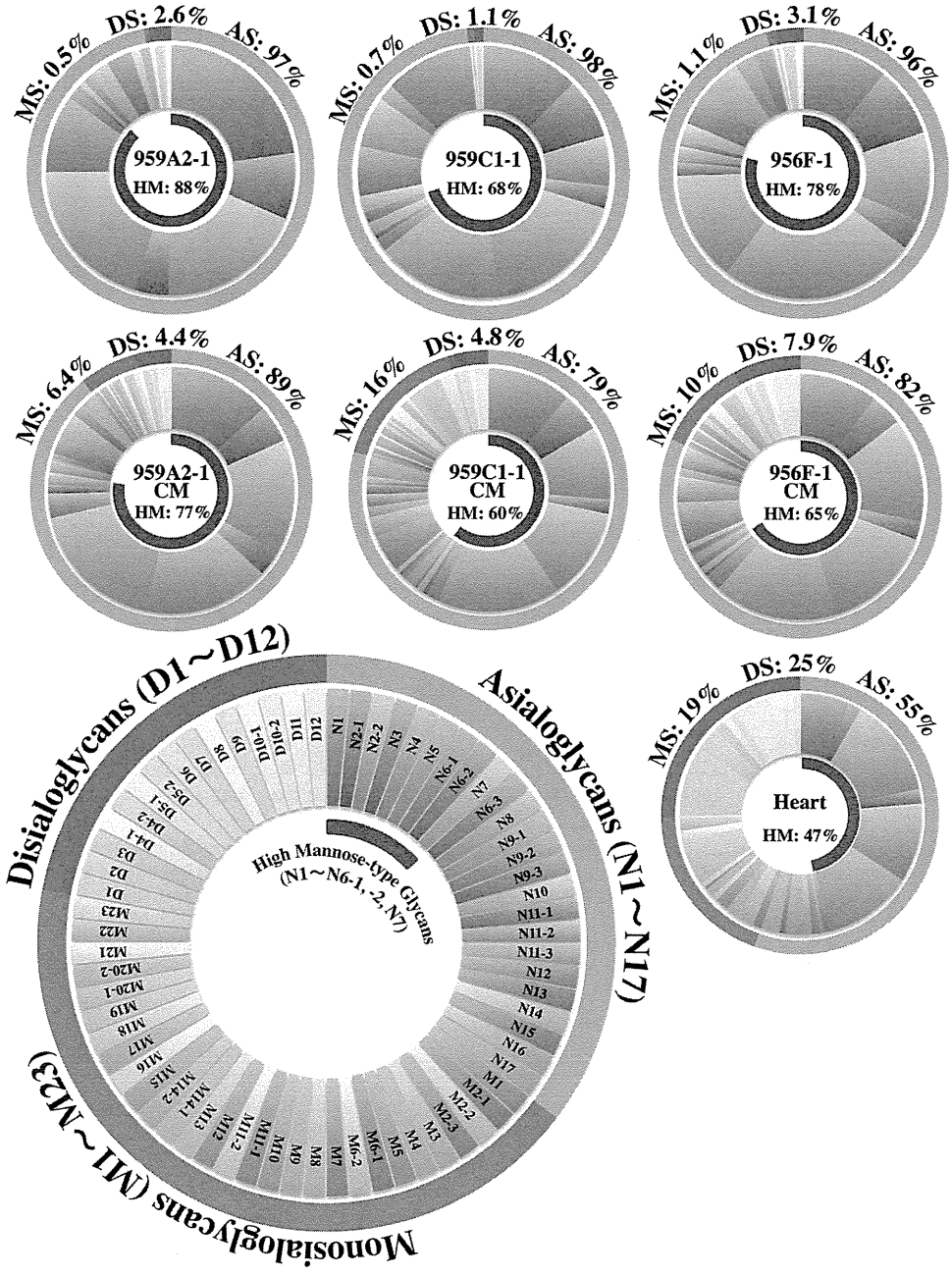

Figure 9. Relative quantities of neutral, monosialyl, and disialyl PA-oligosaccharides in iPSCs, iPSC-CM, and heart cells. Relative quantities of each glycan, calculated from the peak area in Figure 5, 6 and 7 vs. total *N*-glycan content in each cell, were expressed in the doughnut charts. Relative quantities of the asialoglycans, the monosialoglycans and the disialoglycans were showed outside of the charts, and relative quantities of the high mannose type glycans were showed inside of the charts. Asialoglycan (AS): the total volume of N1-N17; Monosialoglycan (MS): the total volume of M1-M23; Disialoglycan (DS): the total volume of D1-D12, High mannose-type glycan (HM): the total volume of N1–N6-1, N6-2, N7.
doi:10.1371/journal.pone.0111064.g009

structures. If human iPSCs or iPSC-CMs do not express CMAH in the same way as murine iPSCs or iPSC-CMs, there may be no difference between human iPSCs, iPSC-CMs, and the human Heart. Further study on human iPSC-CM will be needed to completely understand the features of the sialyl acid of *N*-glycans.

It was reported that human iPSCs produced α2,6sialyl glycans but did not contain α2,3sialyl structures, in contrast to human fibroblast, the origin of iPSCs, which produced α2,3sialyl but not α2,6sialyl structures [30,31]. The murine iPSCs in this study contained α2,3sialyl structures in NeuAc, M5, M23, D4-1, D10-1 and D12, and the iPSC-CMs produced α2,3 and α2,6sialyl structures in NeuAc. These differences may be due to variations between species, because mouse Heart cells also contained α2,3 and α2,6sialyl structures in NeuGc. Further studies are needed to characterize the glycome shift in the production and differentiation of iPSCs.

Type I Lactose structures were not detected, although over 98% of glycans in each cell were accounted for in this study. The *N*-glycans of N9-3, M8, M12, M17, and M23, which were identified after α-galactosidase digestion, contained Galα1-6Gal, not only in

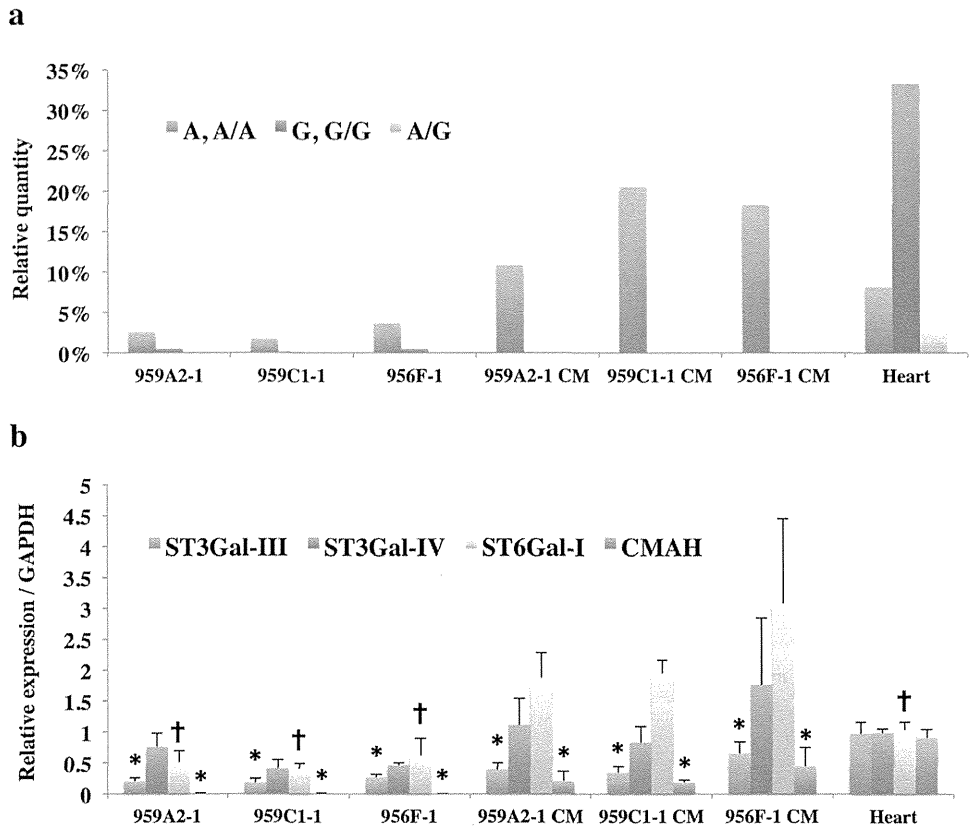

Figure 10. Rarely expressed NeuGc-containing glycans in iPSCs and iPSC-CMs. (a) Relative quantities of NeuAc- and NeuGc-containing glycans; Monosialoglycans containing NeuAc and Disialoglycans containing two NeuAc (A, A/A): the total volume of M1, M2-1, M2-2, M5-M8, M10-M14, M16-M19, M20-2, M21-M23, D4-1, D4-2, D6, D7, D9, D10-1, D12, Disialoglycan containing NeuAc and NeuGc (A/G): D11, Monosialoglycan containing NeuGc and Disialoglycan containing two NeuGc (G, G/G): the total volume of M2-3, M3, M4, M9, M15, M20-1, D1-D3, D5-1, D5-2, D8, D10-2. (b) Transcript expression of ST3Gal-III, ST3Gal-IV, ST6Gal-I, and CMAH; Transcript expression of glycosyltransferases in iPSCs, iPSC-CM, and heart cells was analyzed by real-time PCR. Results are expressed as the mean ± standard deviation. *P<0.05 vs. Heart, †P<0.05 vs. iPSC-CM (all of the 959A2-1 CM, 959C1-1 CM and 956F-1 CM).
doi:10.1371/journal.pone.0111064.g010

the neutral glycans but also in the monosialyl *N*-glycans of the iPSC-CM preparation. The same structure was not found in iPSCs, but only one structure, M23, was present in Heart cells. Therefore, in iPSC-CMs, Galα1-6Gal enzyme activity appears to be up-regulated in comparison to wild-type myocardium, although enzyme activity was not assessed by RT-PCR because of the limited availability of genetic sequence data.

The D8 was identified in all of three iPSC lines and not in the iPSC-CMs and Heart. This structure, unfortunately not identified in this study, may be useful as markers of undifferentiated iPSCs in the same way as well-known pluripotency biomarkers such as stage-specific embryonic antigens (SSEA)-3, SSEA-4 (glycosphingolipids) [32].

Previous MALDI-TOF/MS and MS/MS studies concluded that many kinds of *N*-glycans are found in organs and cells. The number of detected *N*-glycans is attributed to the sensitivity of the MS and HPLC methods employed. That is, MS data are sensitive and can be rapidly obtained, but a glycan structure is identified based only on the calculated molecular weight. Therefore, discriminating between isomeric structures is difficult. On the other hand, it thus appears that the accuracy of the data presented here using HPLC mapping in conjunction with a MALDI-TOF technique provides much more detailed information. Our data were used to identify the representative features of each *N*-glycan in these three cell types.

There may be a concern that the heart tissue used in this study contains connective tissues, vessels or nerves other than cardiomyocytes. Therefore, some of the *N*-glycans detected from the Heart sample might be derived from the tissues other than cardiomyocytes. However, heart is majority composed by cardiomyocytes, and furthermore, even if a small amount of *N*-glycans derived from connective tissues were contaminated in the Heart sample, the main evidences in this study, such as the proportion of the high-mannose type *N*-glycans, the ratio of the active sialyltransferase genes, the existence of NeuGc, and the uncommonness of Galα1-6 Gal, are essentially not affected.

In summary, murine iPSCs were rich in high-mannose type *N*-glycans but very poor in sialyl type *N*-glycans. Murine heart tissue contained a relatively low volume of high-mannose glycans, but was very rich in neuraminic acid, especially NeuGc type sialyl structures. Under these conditions, the volume of each type of glycan was similar for iPSC-CMs and iPSCs. That is, they were rich in high-mannose and relatively poor in sialyl type *N*-glycans by volume. In addition, most of the sialyl structures of the iPSC-CMs were different from those of the Heart, and the iPSC-CMs expressed no NeuGc. Moreover, the iPSC-CMs produced several unique glycans with the Galα1-6Gal structure. These results

provide important data that can be useful in future clinical iPSC studies.

It is quite important to investigate the meaning of *N*-glycans transitions during the cardiomyogenic differentiation presented in this study, for deeply understanding the relationship between the *N*-glycan expression and cardiomyogenic differentiation. Knock-out or knock-down of the genes related to cardiomyogenic differentiation or glycosylation may be useful for such purpose. However, the *N*-glycan signature in the cell surface is determined by a variety of the genes. Knock-out or knock-down of a single gene related to cardiomyogenic differentiation would alter an array of gene expressions, such as sarcomere proteins, transcriptional factors, or cell surface proteins, all of which would affect the signature of *N*-glycans in the cell surface. Therefore, the data interpretation for relationship between expression of a single gene and *N*-glycan signature would be difficult. Some different experimental approach may be needed to investigate the meaning of change in *N*-glycan expression during cardiomyogenic differentiation.

Supporting Information

Table S1 Structures and relative quantities of neutral (Table S1, S2) PA-oligosaccharides derived from iPSC, iPSC-CM, and heart cells. a. Glucose units (GU) were calculated from the peak elution times of the peaks obtained from the ODS column in Figure 5, 6, 7 and the Amide column (data not shown). b. Average mass calculated from the *mlz* values of $[M+Na]^+$ or $[M+H]^+$ ion for neutral, $[M-H]^-$ ion for mono-sialyl, and $[M-H]^-$ & $[M+Na-2H]^-$ ions for di-sialyl PA-oligosaccharides. c. PA-oligosaccharide structures. d. mol% was calculated from the peak area versus total *N*-glycan content in each cell
(TIFF)

Table S2 Structures and relative quantities of neutral (Table S1, S2) PA-oligosaccharides derived from iPSC, iPSC-CM, and heart cells.
(TIFF)

Table S3 Structures and relative quantities of mono-sialyl (Table S3, S4) PA-oligosaccharides derived from iPSC, iPSC-CM, and heart cells.
(TIFF)

Table S4 Structures and relative quantities of mono-sialyl (Table S3, S4) PA-oligosaccharides derived from iPSC, iPSC-CM, and heart cells.
(TIFF)

Table S5 Structures and relative quantities of disialyl PA-oligosaccharides derived from iPSC, iPSC-CM, and heart cells.
(TIFF)

Video S1
(MP4)

Acknowledgments

Our deepest appreciation goes to Professor Shinya Yamanaka and Keisuke Okita of the Center for iPS Cell Research and Application, Kyoto University, who kindly provided the murine iPSCs. We also thank Sachiko Kondo and Uichiro Yabe of MBL, Nagoya, Japan, who gave invaluable comments regarding *N*-glycan analysis.

Author Contributions

Conceived and designed the experiments: TK S. Miyagawa S. Miyagawa JL YS. Performed the experiments: TK AY NK AK EI AM HE KT. Analyzed the data: TK S. Miyagawa YS. Contributed reagents/materials/analysis tools: TK AY JL. Wrote the paper: TK S. Miyagawa YS SF. Obtained permission for use of cell line: S. Miyagawa AS YS.

References

1. Gonzales C, Pedrazzini T (2009) Progenitor cell therapy for heart disease. Exp Cell Res 315: 3077–3085.
2. Shah AM, Mann DL (2011) In search of new therapeutic targets and strategies for heart failure: recent advances in basic science. Lancet 378: 704–712.
3. Yoshida Y, Yamanaka S (2010) Recent stem cell advances: induced pluripotent stem cells for disease modeling and stem cell-based regeneration. Circulation 122: 80–87.
4. Yoshida Y, Yamanaka S (2011) iPS cells: A source of cardiac regeneration. Journal of Molecular and Cellular Cardiology 50: 327–332.
5. Kawamura M, Miyagawa S, Miki K, Saito A, Fukushima S, et al. (2012) Feasibility, safety, and therapeutic efficacy of human induced pluripotent stem cell-derived cardiomyocyte sheets in a porcine ischemic cardiomyopathy model. Circulation 126: S29–37.
6. Mercola M, Colas A, Willems E (2013) Induced pluripotent stem cells in cardiovascular drug discovery. Circ Res 112: 534–548.
7. Sinnecker D, Goedel A, Laugwitz KL, Moretti A (2013) Induced pluripotent stem cell-derived cardiomyocytes: a versatile tool for arrhythmia research. Circ Res 112: 961–968.
8. Kamakura T, Makiyama T, Sasaki K, Yoshida Y, Wuriyanghai Y, et al. (2013) Ultrastructural maturation of human-induced pluripotent stem cell-derived cardiomyocytes in a long-term culture. Circ J 77: 1307–1314.
9. Kuzmenkin A, Liang H, Xu G, Pfannkuche K, Eichhorn H, et al. (2009) Functional characterization of cardiomyocytes derived from murine induced pluripotent stem cells in vitro. FASEB J 23: 4168–4180.
10. Varki A (1993) Biological roles of oligosaccharides: all of the theories are correct. Glycobiology 3: 97–130.
11. Haltiwanger RS, Lowe JB (2004) Role of glycosylation in development. Annu Rev Biochem 73: 491–537.
12. Ohtsubo K, Marth JD (2006) Glycosylation in cellular mechanisms of health and disease. Cell 126: 855–867.
13. Surani MA (1979) Glycoprotein synthesis and inhibition of glycosylation by tunicamycin in preimplantation mouse embryos: compaction and trophoblast adhesion. Cell 18: 217–227.
14. Akama TO, Nakagawa H, Sugihara K, Narisawa S, Ohyama C, et al. (2002) Germ cell survival through carbohydrate-mediated interaction with Sertoli cells. Science 295: 124–127.
15. Hato M, Nakagawa H, Kurogochi M, Akama TO, Marth JD, et al. (2006) Unusual N-glycan structures in alpha-mannosidase II/IIx double null embryos identified by a systematic glycomics approach based on two-dimensional LC mapping and matrix-dependent selective fragmentation method in MALDI-TOF/TOF mass spectrometry. Mol Cell Proteomics 5: 2146–2157.
16. Lau KS, Partridge EA, Grigorian A, Silvescu CI, Reinhold VN, et al. (2007) Complex N-glycan number and degree of branching cooperate to regulate cell proliferation and differentiation. Cell 129: 123–134.
17. Kraushaar DC, Rai S, Condac E, Nairn A, Zhang S, et al. (2012) Heparan sulfate facilitates FGF and BMP signaling to drive mesoderm differentiation of mouse embryonic stem cells. J Biol Chem 287: 22691–22700.
18. Amano M, Yamaguchi M, Takegawa Y, Yamashita T, Terashima M, et al. (2010) Threshold in stage-specific embryonic glycotypes uncovered by a full portrait of dynamic N-glycan expression during cell differentiation. Mol Cell Proteomics 9: 523–537.
19. Okita K, Nakagawa M, Hyenjong H, Ichisaka T, Yamanaka S (2008) Generation of mouse induced pluripotent stem cells without viral vectors. Science 322: 949–953.
20. Miki K, Uenaka H, Saito A, Miyagawa S, Sakaguchi T, et al. (2012) Bioengineered myocardium derived from induced pluripotent stem cells improves cardiac function and attenuates cardiac remodeling following chronic myocardial infarction in rats. Stem Cells Transl Med 1: 430–437.
21. Yu T, Miyagawa S, Miki K, Saito A, Fukushima S, et al. (2013) In vivo differentiation of induced pluripotent stem cell-derived cardiomyocytes. Circ J 77: 1297–1306.
22. Tohyama S, Hattori F, Sano M, Hishiki T, Nagahata Y, et al. (2013) Distinct metabolic flow enables large-scale purification of mouse and human pluripotent stem cell-derived cardiomyocytes. Cell Stem Cell 12: 127–137.
23. Takahashi N, Khoo KH, Suzuki N, Johnson JR, Lee YC (2001) N-glycan structures from the major glycoproteins of pigeon egg white: predominance of terminal Galalpha(1)Gal. J Biol Chem 276: 23230–23239.

24. Takahashi N, Kato K (2003) GALAXY(Glycoanalysis by the Three Axes of MS and Chromatography): a Web Application that Assists Structural Analyses of N-Glycans. Trends in Glycoscience and Glycotechnology 15 No.84: 235–251.
25. Yagi H, Takahashi N, Yamaguchi Y, Kimura N, Uchimura K, et al. (2005) Development of structural analysis of sulfated N-glycans by multidimensional high performance liquid chromatography mapping methods. Glycobiology 15: 1051–1060.
26. Dalziel M, Crispin M, Scanlan CN, Zitzmann N, Dwek RA (2014) Emerging principles for the therapeutic exploitation of glycosylation. Science 343: 1235681.
27. Varki A (2009) Multiple changes in sialic acid biology during human evolution. Glycoconj J 26: 231–245.
28. Irie A, Koyama S, Kozutsumi Y, Kawasaki T, Suzuki A (1998) The molecular basis for the absence of N-glycolylneuraminic acid in humans. J Biol Chem 273: 15866–15871.
29. Chou HH, Takematsu H, Diaz S, Iber J, Nickerson E, et al. (1998) A mutation in human CMP-sialic acid hydroxylase occurred after the Homo-Pan divergence. Proc Natl Acad Sci U S A 95: 11751–11756.
30. Hasehira K, Tateno H, Onuma Y, Ito Y, Asashima M, et al. (2012) Structural and quantitative evidence for dynamic glycome shift on production of induced pluripotent stem cells. Mol Cell Proteomics 11: 1913–1923.
31. Tateno H, Toyota M, Saito S, Onuma Y, Ito Y, et al. (2011) Glycome diagnosis of human induced pluripotent stem cells using lectin microarray. J Biol Chem 286: 20345–20353.
32. Fujitani N, Furukawa J, Araki K, Fujioka T, Takegawa Y, et al. (2013) Total cellular glycomics allows characterizing cells and streamlining the discovery process for cellular biomarkers. Proc Natl Acad Sci U S A 110: 2105–2110.